Available online at www.eccomasproceedia.org
Eccomas Proceedia COMPDYN (2017) 1259-1296

ECCOMAS
Proceedia

COMPDYN 2017
6th ECCOMAS Thematic Conference on
Computational Methods in Structural Dynamics and Earthquake Engineering
M. Papadrakakis, M. Fragiadakis (eds.)
Rhodes Island, Greece, 15–17 June 2017

AN ERROR INDICATOR BASED ON A WAVE DISPERSION ANALYSIS FOR THE IN-PLANE VIBRATION MODES OF ISOTROPIC ELASTIC SOLIDS DISCRETIZED BY ENERGY-ORTHOGONAL FINITE ELEMENTS

Francisco José Brito Castro

Departamento de Ingeniería Industrial, Universidad de La Laguna
Calle Méndez Núñez 67-2C, Santa Cruz de Tenerife 38001, Spain
e-mail: fjbrito@ull.es

Keywords: energy-orthogonal stiffness, numerical dispersion, vibration eigenmodes.

Abstract. *This paper studies the dispersion of elastic waves in homogeneous and isotropic elastic media discretized by the finite element method. Both the unbounded plain-strain solid and the unbounded generalized plane-stress plate are considered. The element stiffness matrix is split into basic and higher order components which are respectively related to the mean and deviatoric components of the element strain field. This decomposition is applied to the elastic energy of the finite element assemblage. By the dispersion analysis the percentage of higher order elastic energy is related to the elastic energy error for both the longitudinal waves and the shear waves. An averaged correlation is proposed to apply the percentage of higher order elastic energy as an error indicator for the vibration eigenmodes computed.*

Peer-review under responsibility of the organizing committee of COMPDYN 2017.
doi: 10.7712/120117.5491.17688

1 INTRODUCTION

It is well known that the wave scattering at boundaries creates an interference field that, if composed solely of waves of frequency equal to a natural frequency of the solid, takes the form of a standing-wave field which is an eigenmode of the continuum [1]. The question of the spatial convergence of the eigenmodes computed by the finite element method is approached in this contribution for the in-plane motion of homogeneous and isotropic elastic solids.

For a plane-strain solid the eigenmodes could be considered essentially composed of longitudinal waves (P) and transverse shear waves (S). Both waves propagate without interaction in the bulk of the material with the respective velocities [2, 3]

$$c_L = ((\lambda + 2\mu)/\rho)^{1/2}, \quad c_T = (\mu/\rho)^{1/2} \tag{1}$$

where: μ, shear modulus of the material; λ Lamé constant of the material; ρ, mass density per unit volume of the material.

The elastic constants λ and μ can be related by

$$\lambda = 2\mu\nu/(1-2\nu) \tag{2}$$

where: ν, the Poisson´s ratio for the material, $0 < \nu < 1/2$.

The elastic constants λ and μ can be obtained from the more familiar engineering Young's modulus E and the Poisson´s ration ν by $\lambda = \nu E/((1+\nu)(1-2\nu))$ and $\mu = E/(2(1+\nu))$.

Similarly, for a generalized plane-stress plate the eigenmodes could be considered essentially composed of longitudinal waves (PL) based on the elementary Poisson theory for the stretching and horizontal shear waves (SH0). Both non dispersive waves propagate without interaction with the respective velocities

$$c_{PL} = 2c_T(1-\alpha^{-1})^{1/2}, \quad c_{SH} = c_T \tag{3}$$

where:

$$\alpha = c_L^2/c_T^2 = (2-2\nu)/(1-2\nu) \tag{4}$$

In each case the longitudinal waves and the shear waves are coupled on the boundary of the elastic medium, an obvious consequence of satisfying the boundary conditions.

For the finite element eigenmodes we suppose that the effect of the spatial discretization over the waves prevails over the effect of the discretization over the scattering at boundaries. In this case, the goal of determining the finite element mesh required to accurately represent a given number of eigenmodes could be approached by analysing the effect of the discretization over the propagation of both the longitudinal waves and the shear waves. The effect of the discretization over the propagation of the above mentioned waves becomes apparent by observing a dispersive behaviour, a phenomenon that is not present in the physical system [4], the analysis of which will be a subject of research in this paper. A survey of computational aspects of wave problems in solids can be found in reference [5]. Recent research about this topic can be found in references [6, 7].

1.1 Governing equations

Let Ω designates the bounded domain with closed boundary ∂Ω occupied by a solid in plane strain parallel to the XY-plane at equilibrium, the Hooke`s law and the strain-displacement relation will be

$$\boldsymbol{\sigma} = 2\mu\boldsymbol{\varepsilon} + \lambda\varepsilon_v\mathbf{I}, \quad \varepsilon_v = div\mathbf{u} \tag{5}$$

$$\boldsymbol{\varepsilon} = \tfrac{1}{2}[grad\mathbf{u} + (grad\mathbf{u})^t] \tag{6}$$

where: $\mathbf{u}:(u_x,u_y)$, displacement vector; ε_v, volumetric strain; $\boldsymbol{\sigma}:\begin{pmatrix}\sigma_{nx} & \tau_{xy}\\ \tau_{xy} & \sigma_{ny}\end{pmatrix}$, Cauchy stress tensor; $\boldsymbol{\varepsilon}:\begin{pmatrix}\varepsilon_{xx} & \varepsilon_{xy}\\ \varepsilon_{xy} & \varepsilon_{yy}\end{pmatrix}$, Cauchy strain tensor

For a plate in generalized plane stress parallel to the XY-plane, the Hooke`s law Eq. (5) is replaced by [8]

$$\boldsymbol{\sigma} = 2\mu\boldsymbol{\varepsilon} + \bar{\lambda}\varepsilon_v\mathbf{I} \tag{7}$$

where:

$$\bar{\lambda} = 2\lambda\mu/(\lambda+2\mu) \tag{8}$$

In both cases, the governing equation of motion (the body forces are neglected) will be,

$$div\boldsymbol{\sigma}(\mathbf{r},t) - \rho\,\partial^2\mathbf{u}(\mathbf{r},t)/\partial t^2 = \mathbf{0}, \quad \mathbf{r}\in\Omega \tag{9}$$

where: t, time coordinate.

To complete a solution, the differential equation Eq. (9) requires specifying boundary conditions. For a solid fixed on a part Σ of its boundary $\partial\Omega$, we have,

$$\mathbf{u}(\mathbf{r},t) = \mathbf{0}, \quad \mathbf{r}\in\Sigma \tag{10}$$

For a given surface force density $\mathbf{f}(\mathbf{r},t)$ on $\Gamma = \partial\Omega \setminus \Sigma$, we have,

$$\boldsymbol{\sigma}(\mathbf{r},t)\mathbf{n}_\perp(\mathbf{r}) = \mathbf{f}(\mathbf{r},t), \quad \mathbf{r}\in\Gamma \tag{11}$$

where: $\mathbf{n}_\perp$, unitary normal external to the boundary $\partial\Omega$.

Finally, the above equations must be completed by the initial conditions of Cauchy on $\mathbf{u}(\mathbf{r},0)$ and $\partial\mathbf{u}(\mathbf{r},t)/\partial t\big|_{t=0}$ in Ω.

For a solid in plane strain parallel to the XY-plane, by considering Eq. (5) the relationship between stresses and engineering strains can be expressed in matrix form as

$$(\sigma_x,\sigma_y,\tau_{xy})^t = \mathbf{E}(\varepsilon_x,\varepsilon_y,\gamma_{xy})^t \tag{12}$$

where: $\mathbf{E}$, elasticity matrix with the non-null components,

$$E_{11} = E_{22} = \lambda + 2\mu, \quad E_{33} = \mu, \quad E_{12} = E_{21} = \lambda \tag{13}$$

By considering Eq. (1) and (4), the elasticity matrix Eq. (13) can be alternatively expressed in the forms,

$$\mathbf{E} = \rho c_L^2\mathbf{E}_L^0(\nu), \quad \mathbf{E} = \rho c_T^2\mathbf{E}_T^0(\nu) \tag{14}$$

Either of $\mathbf{E}_L^0(\nu)$ and $\mathbf{E}_T^0(\nu)$ is called the dimensionless elasticity matrix for plane strain. These matrices have the following non-null components,

$$E_{L,11}^0 = E_{L,22}^0 = 1, \quad E_{L,33}^0 = \alpha^{-1}, \quad E_{L,12}^0 = E_{L,21}^0 = 1 - 2\alpha^{-1} \tag{15}$$

$$E_{T,11}^0 = E_{T,22}^0 = \alpha, \quad E_{T,33}^0 = 1, \quad E_{T,12}^0 = E_{T,21}^0 = \alpha - 2 \tag{16}$$

For a plate in generalized plane stress parallel to the XY-plane, by considering Eq. (7) the elasticity matrix will has the non-null components,

$$E_{11} = E_{22} = \bar{\lambda} + 2\mu, \quad E_{33} = \mu, \quad E_{12} = E_{21} = \bar{\lambda} \tag{17}$$

By considering Eq. (1), (3), (4) and (8), the elasticity matrix Eq. (17) can be alternatively expressed in the forms,

$$\mathbf{E} = \rho c_{PL}^2 \mathbf{E}_{PL}^0(\nu), \quad \mathbf{E} = \rho c_{SH}^2 \mathbf{E}_{SH}^0(\nu) \tag{18}$$

Either of $\mathbf{E}_{PL}^0(\nu)$ and $\mathbf{E}_{SH}^0(\nu)$ is called the dimensionless elasticity matrix for generalized plane stress. These matrices have the following non-null components,

$$E_{PL,11}^0 = E_{PL,22}^0 = 1, \quad E_{PL,33}^0 = (4(1-\alpha^{-1}))^{-1}, \quad E_{PL,12}^0 = E_{PL,21}^0 = (1-2\alpha^{-1})/(2(1-\alpha^{-1})) \tag{19}$$

$$E_{SH,11}^0 = E_{SH,22}^0 = 4(1-\alpha^{-1}), \quad E_{SH,33}^0 = 1, \quad E_{SH,12}^0 = E_{SH,21}^0 = 2(1-2\alpha^{-1}) \tag{20}$$

In a plane-strain solid, the forms of the elasticity matrix given by Eq. (14) will be useful to analyze the propagation of longitudinal waves (P) and transverse shear waves (S), respectively. Similarly, in a generalized plane-stress plate, Eq. (18) will be useful to analyze the propagation of longitudinal waves (PL) and horizontal shear waves (SH0).

For time-harmonic waves, time may be removed from the problem by writing

$$\mathbf{u} = \tilde{\mathbf{u}}(\mathbf{r}) \exp(-i\omega t), \quad \mathbf{r} \in \Omega \tag{21}$$

where: $\tilde{\mathbf{u}}(\mathbf{r})$, complex amplitude of the wave; $\omega = 2\pi/T$, circular frequency; T, period of wave.

By considering Eq. (21) and Eq. (6), for the Cauchy stress tensor Eq. (5) or Eq. (7) we obtain

$$\boldsymbol{\sigma} = \tilde{\boldsymbol{\sigma}}(\mathbf{r}) \exp(-i\omega t), \quad \mathbf{r} \in \Omega \tag{22}$$

where: $\tilde{\boldsymbol{\sigma}}(\mathbf{r})$, complex amplitude of the Cauchy stress tensor.

Similarly, for the surface force density,

$$\mathbf{f} = \tilde{\mathbf{f}}(\mathbf{r}) \exp(-i\omega t), \quad \mathbf{r} \in \Gamma \tag{23}$$

where: $\tilde{\mathbf{f}}(\mathbf{r})$, complex amplitude of surface force density.

Inserting the time-harmonic dependence Eq. (21) - (23) into the Eq. (9) - (11), the boundary value problem is then written

$$div\tilde{\boldsymbol{\sigma}}(\mathbf{r}) + \rho\omega^2 \tilde{\mathbf{u}}(\mathbf{r}) = \mathbf{0}, \quad \mathbf{r} \in \Omega \tag{24}$$

$$\tilde{\mathbf{u}}(\mathbf{r}) = \mathbf{0}, \quad \mathbf{r} \in \Sigma \tag{25}$$

$$\tilde{\boldsymbol{\sigma}}(\mathbf{r})\mathbf{n}_{\perp}(\mathbf{r}) = \tilde{\mathbf{f}}(\mathbf{r}), \quad \mathbf{r} \in \Gamma \tag{26}$$

1.2 Finite element formulation

The boundary value problem Eq. (24) - (26) is posed in variational form [9]

$$\int_{\Omega} (\boldsymbol{\sigma} : \delta\boldsymbol{\varepsilon} - \omega^2 \rho \mathbf{u} \cdot \delta\mathbf{u}) dV = \int_{\Gamma} (\mathbf{f} \cdot \delta\mathbf{u}) dS \tag{27}$$

The variational form Eq. (27) is discretized by the finite element method yielding the following matrix expression

$$(\mathbf{K} - \omega^2 \mathbf{M})\mathbf{x} = \mathbf{F} \tag{28}$$

where: **K**, global stiffness matrix; **M**, global mass matrix; **x**, column matrix containing the nodal displacement of the finite element assemblage; **F**, column matrix of nodal external load.

Defining at element level the matrix $\mathbf{B}^e$ relating the engineering strain components to the nodal values of displacement,

$$\mathbf{e}^e = \mathbf{B}^e \mathbf{x}^e \tag{29}$$

and considering the matrix relationship between engineering strains and stresses Eq. (12), the element stiffness matrix is then written $\mathbf{K}^e = \int_{\Omega e} (\mathbf{B}^e)^t \mathbf{E} \mathbf{B}^e dV$.

The elastic energy of the solid occupying the bounded domain Ω will be

$$E_0 = \tfrac{1}{2} \int_\Omega \mathrm{Re}[\boldsymbol{\sigma}] : \mathrm{Re}[\boldsymbol{\varepsilon}] dV \tag{30}$$

For the discretized domain, the energy at element level is yielded by inserting Eq. (29) and (12) into the matrix form of Eq. (30). The elastic energy of the finite element assemblage will be the sum of the element energies. Then,

$$E = \tfrac{1}{2} \mathrm{Re}[\mathbf{x}^t] \mathbf{K} \, \mathrm{Re}[\mathbf{x}] \tag{31}$$

1.2.1 Energy-orthogonal decomposition

The matrix relating the engineering strain components to the nodal values of displacement at element level Eq. (29) is partitioned into mean and deviatoric components, $\mathbf{B}^e = \overline{\mathbf{B}}^e + \mathbf{B}_d^e$, where $\overline{\mathbf{B}}^e V^e = \int_{\Omega e} \mathbf{B}^e dV$ and $\mathbf{B}_d^e = \mathbf{B}^e - \overline{\mathbf{B}}^e$. The element stiffness matrix is then written,

$$\mathbf{K}^e = \mathbf{K}_b^e + \mathbf{K}_h^e \tag{32}$$

where: $\mathbf{K}_b^e = \int_{\Omega e} (\overline{\mathbf{B}}^e)^t \mathbf{E} \overline{\mathbf{B}}^e dV$, basic stiffness matrix; $\mathbf{K}_h^e = \int_{\Omega e} (\mathbf{B}_d^e)^t \mathbf{E} \mathbf{B}_d^e dV$, higher order stiffness matrix.

In this case it is said that the element stiffness matrix is decomposed in energy-orthogonal form [10]. The concept of energy-orthogonal stiffness matrix regarded in this paper was explicitly introduced in the context of the linear elasticity by Bergan and Nygärd within the framework of the Free Formulation [11], and by Felippa within the framework of the Parametrized Variational Principles [12].

The decomposition in Eq. (32) holds for the complete model whenever $\mathbf{K}_b^e$ and $\mathbf{K}_h^e$ are independently assembled,

$$\mathbf{K} = \mathbf{K}_b + \mathbf{K}_h \tag{33}$$

Inserting Eq. (33) into Eq. (31), we obtain the basic and higher order elastic energies of the finite element assemblage.

1.2.2 Stationary waves

For a stationary wave, the amplitude of displacement is a real-valued vector. Then, from Eq. (31), the period-averaged elastic energy for the discretized domain will be

$$\overline{E} = \tfrac{1}{2} \widetilde{\mathbf{x}}^t \mathbf{K} \widetilde{\mathbf{x}} \int_0^1 \cos^2(2\pi\tau) d\tau = \tfrac{1}{4} \widetilde{\mathbf{x}}^t \mathbf{K} \widetilde{\mathbf{x}} \tag{34}$$

where: $\tau = t/T$, $0 \le \tau \le 1$, dimensionless time; $\widetilde{\mathbf{x}}$, column matrix containing the real nodal amplitudes of displacement.

By introducing the decomposition in Eq. (33) into Eq. (34) we obtain the basic and higher order period-averaged elastic energies. The latter component will be

$$\overline{E}_h = \tfrac{1}{4}\widetilde{\mathbf{x}}^t \mathbf{K}_h \widetilde{\mathbf{x}} \tag{35}$$

1.3 Scope of research

In this contribution the dispersion properties and the density of period-averaged elastic energy are computed for non-dispersive plane harmonic waves in unbounded plane-strain solids and unbounded generalized plane-stress plates discretized by regular meshes of energy-orthogonal finite elements. Given the mesh, in the limit of long wavelength, although the elastic energy density does not vanish, its higher order component does vanish. Similarly, given the wavelength, as the solution converges on account of mesh refinement, the elastic energy density is increasingly dominated by its basic component. The above heuristic argument motivates to research the relationship between the higher order elastic energy and the elastic energy error in order to explore the behaviour of this energy component as an error indicator. To be precise, by the dispersion analysis, an averaged correlation between the percentage of higher order elastic energy and the elastic energy error will be yielded versus the Poisson's ratio for both longitudinal and shear waves. The use of both correlations as reference to apply the higher order elastic energy as an error indicator for the elastic vibration modes computed by the finite element method will be explored. A similar correlation has been proposed for acoustic waves in fluid media [13]. Arguments to support the higher order energy as an error indicator in the context of the linear elasticity have already been established [12].

2 DISPERSION ANALYSIS

2.1 Characteristic equations

The unbounded plane-strain solid and the unbounded generalized plane-stress plate are discretized by a regular mesh of finite elements. Two different standard isoparametric finite elements are considered [14]: the eight nodes quadrilateral with parallelogram geometry QU8, and the six nodes triangle with isosceles geometry TR6, Fig. 1. The nodal lattice formed by the finite element assemblage has three and four nodes per unit cell, respectively. Different meshes with the same element area are yielded by the aspect ratio parameter γ, where $0 < \gamma \leq 1$; additionally, for the QU8 element, the skew angle β also can be selected, where $0 \leq \beta < 90^{\circ}$. The finite element analysis will be performed by using the rectangular coordinate system XY.

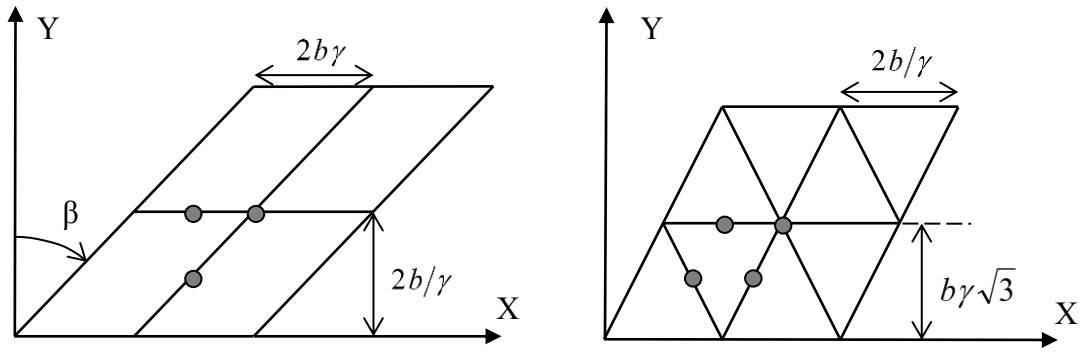

Figure 1: Regular mesh of eight nodes quadrilateral elements and regular mesh of six nodes triangular elements with unit cells

For uniform plane harmonic waves,

$$\begin{gathered}\tilde{\mathbf{u}}(\mathbf{r}) = A\hat{\mathbf{a}}\exp(i\kappa\mathbf{n}\cdot\mathbf{r}) \\ \mathbf{n} = (\cos\theta, \sin\theta), \quad \mathbf{r} = (x, y)\end{gathered} \tag{36}$$

where: A, amplitude of the wave; $\hat{\mathbf{a}}$, polarization vector, unit vector indicating the direction of the particle displacement; $\mathbf{n}$, wave normal, unit vector indicating the direction of the wave propagation; θ, angle of wave propagation, $0 \le \theta \le 180^{\circ}$; $\kappa = 2\pi/\lambda = \omega/c$, wave number; λ, wavelength; c, phase speed of the continuum.

For the longitudinal plane waves the displacements are in the direction of the wave normal, $\hat{\mathbf{a}} = \mathbf{n}$, and only normal stresses act along the wave front; nevertheless, for the shear plane waves, the displacements are perpendicular to the wave normal, $\hat{\mathbf{a}} \cdot \mathbf{n} = 0$, and only shearing stresses act along the wave front.

For a plane elastic wave Eq. (36) the density of period-averaged elastic energy can be computed by the equation [15]

$$\overline{E}_0 = \tfrac{1}{4}\rho\omega^2 A^2 \tag{37}$$

The characteristic equations can be found assuming harmonic waves Eq. (36) with different amplitudes in each node of the unit cell,

$$\tilde{\mathbf{u}} = A_j\hat{\mathbf{a}}\exp(i\kappa\mathbf{n}\cdot\mathbf{r}), \quad j = 1, \ldots, N \tag{38}$$

where: N, number of nodes per unit cell.

Inserting the solutions Eq. (38) into the homogeneous part of Eq. (28), the characteristic equation for each node of the unit cell is yielded by equilibrium of nodal forces into the direction of the particle displacement [16],

$$\mathbf{F}_K \cdot \hat{\mathbf{a}} - \omega^2 \mathbf{F}_M \cdot \hat{\mathbf{a}} = 0 \tag{39}$$

where: $\mathbf{F}_K$, nodal force associated to the global stiffness matrix; $\mathbf{F}_M$, nodal force associated to the global mass matrix.

By considering Eq. (39) for each node of the unit cell, a homogeneous system of N algebraic equations is formed,

$$\begin{gathered}\mathbf{ZA} = \mathbf{0} \\ z_{ij}A_j = 0, \quad i, j = 1, \ldots, N\end{gathered} \tag{40}$$

$$z_{ij} = a_{ij}(m, \theta, \nu, \boldsymbol{\delta}) + \varpi^2 b_{ij}(m, \theta, \boldsymbol{\delta}) \tag{41}$$

$$m = b\kappa/\pi = 2b/\lambda, \quad \varpi = (2b/c)\,\omega \tag{42}$$

where: m, dimensionless wave number, $0 < m < 1$; b, half of the element size; ϖ, dimensionless frequency of the discretized elastic domain; $\boldsymbol{\delta} = (\gamma, \beta)$ form parameters for the QU8 element, or $\boldsymbol{\delta} = (\gamma)$ form parameter for the TR6 element.

In this procedure, by considering Eq. (14) for the plane-strain solid and Eq. (18) for the generalized plane-stress plate, the global stiffness matrix has been expressed in the suitable form

$$\mathbf{K} = \rho c^2 h \mathbf{K}^0 \tag{43}$$

where: h, thickness of the elastic domain in the Z-direction.

Similarly, the global mass matrix has been suitably expressed as $\mathbf{M} = \rho(2b)^2 h\mathbf{M}^0$

2.2 Dispersion equations

The system of homogeneous algebraic equations given in Eq. (40) has a non-trivial solution only if the matrix **Z** is singular; that is,

$$\det\left[\mathbf{Z}(m,\theta,\nu,\boldsymbol{\delta},\varpi)\right] = 0 \tag{44}$$

From Eq. (44) the following polynomial equation is yielded

$$\sum_{r=0}^{N} c_r q^r = 0, \quad c_N = 1 \tag{45}$$

where: $q = \varpi^2$; $c_r(m,\theta,\nu,\boldsymbol{\delta})$, coefficients obtained from a_{ij} and b_{ij}, Eq. (41).

Either of Eq. (44) and (45) is called the characteristic frequency equation for the plane wave propagation. The zeroes of Eq. (45) are computed in closed form as functions of its coefficients. Then, the components

$$q_k = q_k(c_0,\ldots,c_{N-1}), \quad k = 1,\ldots,N \tag{46}$$

or, alternatively,

$$\varpi_k = \varpi_k(m,\theta,\nu,\boldsymbol{\delta}), \quad k = 1,\ldots,N \tag{47}$$

will be continuous functions precisely defined. Either of Eq. (46) and (47) is called the dispersion equations.

Substituting Eq. (47) into Eq. (40), the wave amplitudes corresponding to the nodes of the unit cell are yielded for each dispersion equation. In this work, each set of linear algebraic equations is numerically solved by using the singular value decomposition method SVD [17].

The range of dimensionless wave number values where each dispersion equation represents the propagation of elastic waves in the discretized medium will be called the acoustical branch of the dispersion equation. In order to determine the acoustical branches, a preliminary constraint condition over the dimension of the null space of **Z** must be imposed,

$$\dim\left[\mathbf{N}(\mathbf{Z})\right] = 1 \tag{48}$$

The constraint condition Eq. (48) implies that the subspace of solutions to Eq. (40) must be one-dimensional. In this case the vector of wave amplitudes **A** is arbitrary to the extent that a scalar multiple of it is also a solution. Then the following constraint conditions are imposed,

$$A_1 = 1; \quad A_j(m,\theta,\nu,\boldsymbol{\delta}) > 0, \quad j = 2,\ldots,N \tag{49}$$

$$(\partial\varpi/\partial m)_{\theta,\nu,\boldsymbol{\delta}} > 0 \tag{50}$$

In molecular physics, condition Eq. (49) is called the restriction of the lattice spectrum to the acoustical branch [18]. Obviously, if the constraint condition Eq. (48) is not imposed, the constraint condition Eq. (49) is meaningless.

From Eq. (42) we obtain both the phase velocity and group velocity of the discretized medium,

$$c_d = c(2\pi)^{-1}\varpi/m \tag{51}$$

$$c_{g,d} = \partial\omega/\partial\kappa = c_g(2\pi)^{-1}\partial\varpi/\partial m \tag{52}$$

where: c_g, group velocity of the continuum.

From Eq. (52), the constraint condition Eq. (50) is equivalent to

$$c_{g,d} > 0 \tag{53}$$

It can be proven that for general periodic motion the energy propagates with the group velocity [2]; therefore, the constraint condition Eq. (53) imposes that the energy propagates into the wave direction. From this point, for each dispersion equation only the acoustical branch will be considered. This one represents the physically admissible solution for mechanical wave propagation.

It must be recall that the group velocity of the continuum will be equal to the phase velocity because the waves propagate non-dispersively. Nevertheless, for the dispersive discretized medium the group velocity will be different from the phase velocity; therefore, the velocity of energy transport will be different from the phase velocity. As a consequence, when we consider the numerical dispersion associated with the finite element spatial discretization, not only the effect over the phase velocity must be analyzed but also the effect over the group velocity or velocity of energy transport.

2.3 Elastic energy at the unit cell

From Eq. (31), (42) and (43) the elastic energy at the unit cell over a period will be

$$E = \tfrac{1}{2}\rho(\omega/\varpi)^2(2b)^2 h\,\mathrm{Re}[\widetilde{\mathbf{x}}^t \exp(-i2\pi\tau)]\,\mathrm{Re}[\widetilde{\mathbf{G}}^0 \exp(-i2\pi\tau)] \tag{54}$$

where: $\mathbf{G}^0 = \widetilde{\mathbf{G}}^0 \exp(-i2\pi\tau)$, column matrix of forces at the nodes of the unit cell, obtained from the stiffness matrix $\mathbf{K}^0$ defined in Eq. (43).

From Eq. (54), the density of period-averaged elastic energy is computed,

$$\overline{E} = \tfrac{1}{4}C\rho(\omega/\varpi)^2 \int_0^1 \mathrm{Re}[\widetilde{\mathbf{x}}^t \exp(-i2\pi\tau)]\,\mathrm{Re}[\widetilde{\mathbf{G}}^0 \exp(-i2\pi\tau)]d\tau \tag{55}$$

where: $C = 2$ for the QU8 element, and $C = 4/\sqrt{3}$ for the TR6 element.

From the decomposition Eq. (33), the density of period-averaged elastic energy Eq. (55) can be partitioned as addition of basic and higher order components. The latter component will be

$$\overline{E}_h = \tfrac{1}{4}C\rho(\omega/\varpi)^2 \int_0^1 \mathrm{Re}[\widetilde{\mathbf{x}}^t \exp(-i2\pi\tau)]\,\mathrm{Re}[\widetilde{\mathbf{G}}_h^0 \exp(-i2\pi\tau)]d\tau \tag{56}$$

From Eq. (56) and (55), the percentage of period-averaged higher order elastic energy can be defined as

$$e_h = \overline{E}_h/\overline{E}, \quad e_h = e_h(m,\theta,\nu,\boldsymbol{\delta}) \tag{57}$$

2.4 Indicators of discretization error

By considering Eq. (51) and (52), the indicators of the dispersion associated with the spatial discretization that is introduced by the finite element model are defined as

$$e_p = c_d/c = (2\pi)^{-1}\varpi/m, \quad e_p = e_p(m,\theta,\nu,\boldsymbol{\delta}) \tag{58}$$

$$e_g = c_{g,d}/c_g = (2\pi)^{-1}\partial\varpi/\partial m, \quad e_g = e_g(m,\theta,\nu,\boldsymbol{\delta}) \tag{59}$$

These indicators consider the effect of the spatial discretization on the wave velocity and the velocity of energy transport, respectively.

From Eq. (55) and (37), the percentage indicator of elastic energy error associated with the spatial discretization that is introduced by the finite element model is defined as

$$\varepsilon = (\overline{E}/\overline{E}_0) - 1, \quad \varepsilon = \varepsilon(m, \theta, \nu, \boldsymbol{\delta}) \tag{60}$$

2.5 Numerical research

Three different meshes having the same element area will be considered both for the QU8 element and the TR6 element. Specifically, Fig. 1:

Q1: square section; $\gamma = 1$, $\beta = 0$.

Q2: rectangular section with aspect ratio 1:2; $\gamma = 1/\sqrt{2}$, $\beta = 0$.

Q3: skewed section; $\gamma = 1$, $\beta = 45^{\circ}$.

T1; triangular section of equilateral geometry, $\gamma = 1$.

T2; triangular section of right geometry, $\gamma^2 = 1/\sqrt{3}$.

T3; triangular section with angle of 30º opposite to the base, $\gamma^2 = \tan 75^{\circ}/\sqrt{3}$.

The indicators Eq. (57) - (60) are computed versus dimensionless wave number for different directions of wave propagation and different values of Poisson´s ratio.

For the unbounded plane-strain solid discretized by the mesh QU8-Q1 and P-waves the indicator of dispersion Eq. (58) is plotted versus dimensionless wave number for two directions of wave propagation in order to represent the anisotropy induced by the spatial discretization, Fig. 2. A discontinuity in phase velocity is observed. In this case the discretized solid medium acts like a band-pass filter [16]. This discontinuity was already described by Brillouin [18] for lattices consisting of different particles.

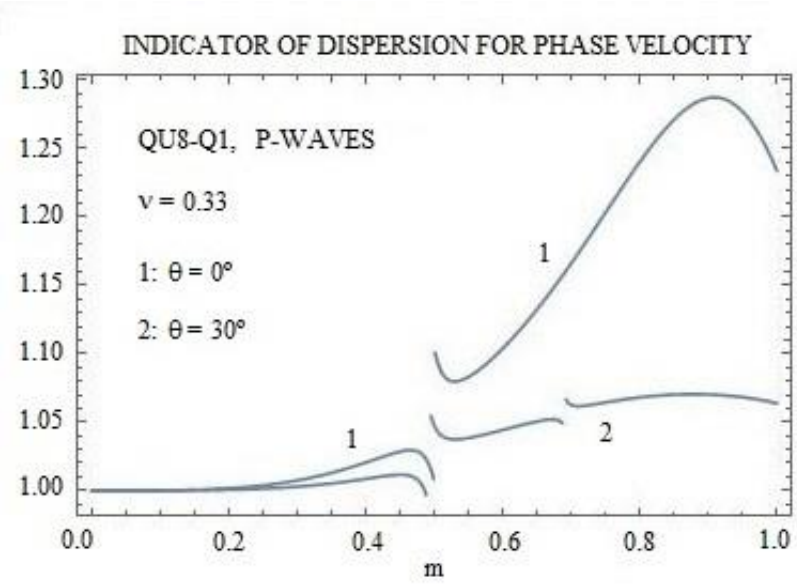

Figure 2: Indicator of dispersion for phase velocity versus dimensionless wave number.

For the unbounded plane-strain solid discretized by the mesh QU8-Q2 and S-waves the indicators Eq. (60) and (57) are plotted versus dimensionless wave number for three directions of wave propagation, Fig. 3 and 4. It is observed that the elastic energy error vanishes both as the mesh is refined and in the limit of long wavelength, as it is expected. Similarly, the density of higher order elastic energy also vanishes both as the mesh is refined and in the limit of long wavelength. This latter behaviour is also expected because the strain field inside each element

becomes uniform. As a conclusion, the dispersion analysis reveals that the higher order elastic energy behaves as an error indicator.

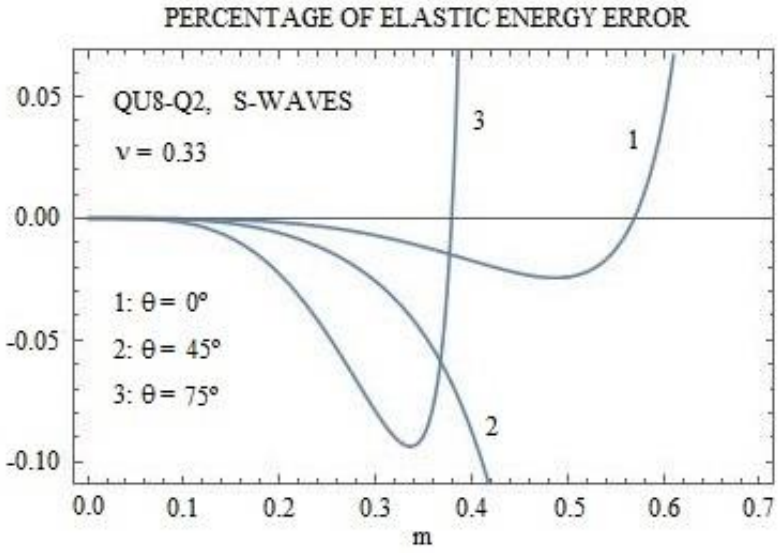

Figure 3: Indicator of elastic energy error versus dimensionless wave number.

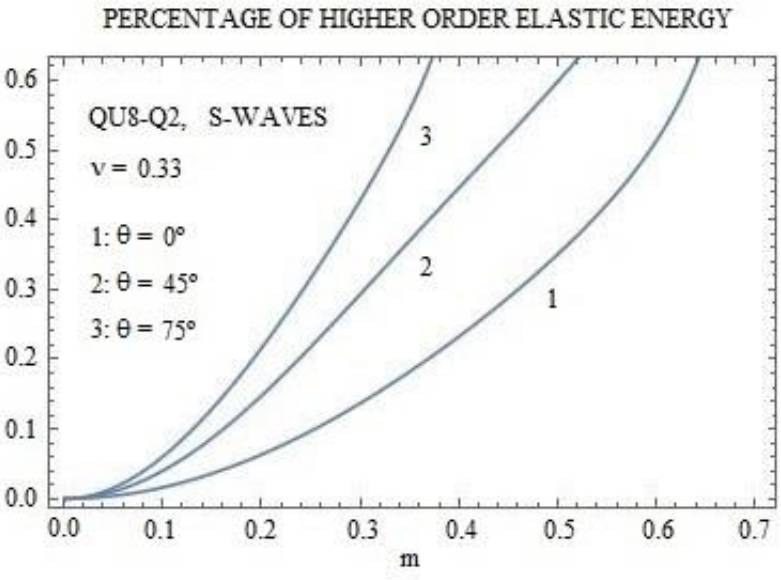

Figure 4: Percentage of higher order elastic energy versus dimensionless wave number.

In this paper an averaged correlation between the percentage of higher order elastic energy and the elastic energy error is pursued. As a first step, from Eq. (57) and (60), a mapping between the elastic energy error and the percentage of higher order elastic energy is defined,

$$\varepsilon = \varepsilon(e_h, \theta, \nu, \boldsymbol{\delta}) \tag{61}$$

For the unbounded plane-strain solid discretized by the mesh QU8-Q2 and S-waves the mapping Eq. (61) is plotted in Fig. 5 for three directions of wave propagation. Similarly, for the unbounded generalized plane-stress plate discretized by the mesh TR6-T3 and PL-waves the mapping Eq. (61) is plotted in Fig. 6 for three directions of wave propagation. In both cases it

is observed that, for moderate values of percentage of higher order elastic energy, this mapping could be approximated by the following cubic correlation,

$$\varepsilon = (A * e_h + B) * e_h^2 \tag{62}$$

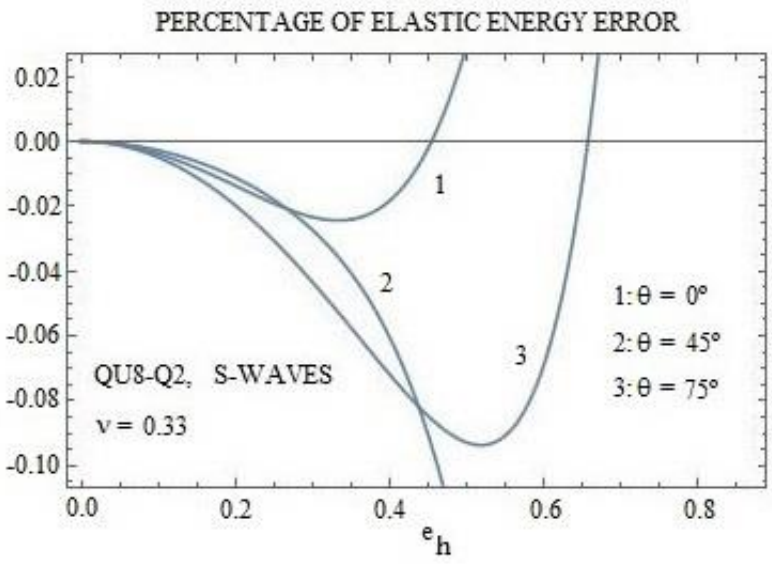

Figure 5: Percentage of elastic energy error versus percentage of higher order elastic energy for QU8 element.

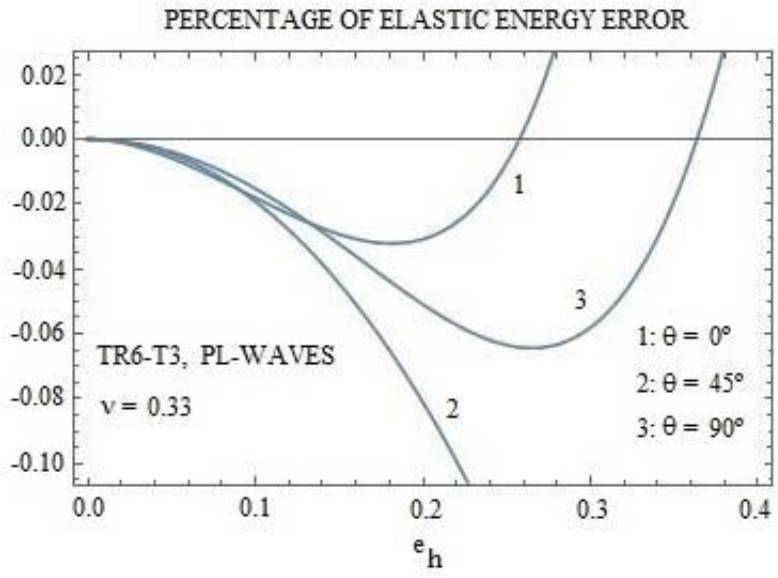

Figure 6: Percentage of elastic energy error versus percentage of higher order elastic energy for TR6 element.

As a second step, for each of the elements considered, two values of percentage of higher order elastic energy Eq. (57) are selected as reference ones,

$$QU8: \quad e_{h1} = 0.10 \quad e_{h2} = 0.20 \tag{63}$$

$$TR6: \quad e_{h1} = 0.045 \quad e_{h2} = 0.09 \tag{64}$$

From Eq. (57), (63) and (64), the first and the second reference dimensionless wave number are defined for each of the elements considered,

$$m_1 = f_{m1}(\theta, \nu, \boldsymbol{\delta}) \tag{65}$$

$$m_2 = f_{m2}(\theta, \nu, \boldsymbol{\delta}) \tag{66}$$

The mean values of Eq. (65) and (66) are computed on the range of propagation angle for each of the test meshes considered and four values of Poisson´s ratio. Mesh averaging of these mean values are displayed for the element QU8 in Table 1 and for the element TR6 in Table 2. The above mesh-averaged values of the first and the second reference dimensionless wave number roughly correspond to six and four elements per wavelength, respectively.

		QU8			
		ν = 0.45	ν = 0.33	ν = 0.25	ν = 0.05
$\overline{m_1^M}$	P	0.1740	0.1742	0.1743	0.1744
	S	0.1742	0.1749	0.1749	0.1749
	PL	0.1743	0.1743	0.1744	0.1744
	SH0	0.1750	0.1749	0.1749	0.1749
$\overline{m_2^M}$	P	0.2526	0.2535	0.2539	0.2542
	S	0.2537	0.2557	0.2558	0.2557
	PL	0.2536	0.2539	0.2540	0.2542
	SH0	0.2557	0.2558	0.2558	0.2557

Table 1: Mesh averaging of the mean values of the first and the second reference dimensionless wave number. Element QU8.

		TR6			
		ν = 0.45	ν = 0.33	ν = 0.25	ν = 0.05
$\overline{m_1^M}$	P	0.1663	0.1662	0.1662	0.1662
	S	0.1651	0.1661	0.1662	0.1663
	PL	0.1662	0.1662	0.1662	0.1662
	SH0	0.1661	0.1662	0.1662	0.1663
$\overline{m_2^M}$	P	0.2408	0.2403	0.2403	0.2402
	S	0.2373	0.2401	0.2403	0.2404
	PL	0.2403	0.2403	0.2403	0.2402
	SH0	0.2402	0.2403	0.2404	0.2404

Table 2: Mesh averaging of the mean values of the first and the second reference dimensionless wave number. Element TR6.

As a third step, from Eq. (60), (65) and (66), the first and the second reference value of percentage of elastic energy error are defined for each of the elements considered,

$$\varepsilon_1 = f_{\varepsilon 1}(\theta, \nu, \boldsymbol{\delta}) \tag{67}$$

$$\varepsilon_2 = f_{\varepsilon 2}(\theta, \nu, \boldsymbol{\delta}) \tag{68}$$

where: $|\varepsilon_1| = |\varepsilon(m)|_{\max}, m \in (0, m_1]$ and $|\varepsilon_2| = |\varepsilon(m)|_{\max}, m \in (0, m_2]$

From Eq. (58), (65) and (66), and from Eq. (59), (65) and (66), reference values can be also defined for the indicators of dispersion associated with the phase and group velocities, respectively. For the second reference values,

$$e_{p2} = f_{ep2}(\theta, \nu, \boldsymbol{\delta}) \tag{69}$$

$$e_{g2} = f_{eg2}(\theta, \nu, \boldsymbol{\delta}) \tag{70}$$

As a fourth step, the root-mean-square values of Eq. (67) and (68) are computed on the range of propagation angle,

$$\varepsilon_1^{RMS}(\nu, \boldsymbol{\delta}) = \sqrt{\tfrac{1}{\pi}\int_0^{\pi} \varepsilon_1^2 d\theta} \tag{71}$$

$$\varepsilon_2^{RMS}(\nu, \boldsymbol{\delta}) = \sqrt{\tfrac{1}{\pi}\int_0^{\pi} \varepsilon_2^2 d\theta} \tag{72}$$

The integrals in Eq. (71) and (72) are computed, for each of the test meshes considered and four values of Poisson´s ratio, by a step of π/180 for the propagation angle. Mesh averaging of these root-mean-square values are displayed for the element QU8 in Table 3 and for the element TR6 in Table 4. By linear interpolation, the above mesh-averaged values can also be obtained for other values of Poisson´s ratio.

QU8					
		ν = 0.45	ν = 0.33	ν = 0.25	ν = 0.05
$\overline{\varepsilon_1^{RMS}}$	P	0.004907	0.003870	0.003598	0.003270
	S	0.003949	0.003105	0.002924	0.002758
	PL	0.003788	0.003593	0.003484	0.003268
	SH0	0.003048	0.002921	0.002859	0.002757
$\overline{\varepsilon_2^{RMS}}$	P	0.027761	0.018764	0.016904	0.014755
	S	0.015603	0.012300	0.011578	0.010960
	PL	0.018198	0.016872	0.016152	0.014739
	SH0	0.012070	0.011567	0.011324	0.010957

Table 3: Mesh averaging of the root-mean-square values of the first and second reference percentage of elastic energy error. Element QU8.

TR6					
		ν = 0.45	ν = 0.33	ν = 0.25	ν = 0.05
$\overline{\varepsilon_1^{RMS}}$	P	0.008718	0.006019	0.005483	0.004930
	S	0.005068	0.004547	0.004407	0.004269
	PL	0.005851	0.005473	0.005279	0.004926
	SH0	0.004504	0.004405	0.004354	0.004268
$\overline{\varepsilon_2^{RMS}}$	P	0.037094	0.025267	0.022893	0.020438
	S	0.019529	0.018347	0.017904	0.017441
	PL	0.024527	0.022852	0.021990	0.020422
	SH0	0.018212	0.017897	0.017729	0.017438

Table 4: Mesh averaging of the root-mean-square values of the first and second reference percentage of elastic energy error. Element TR6.

As a last step, we propose to apply the cubic correlation Eq. (62) to define a mapping that associates an averaged value of percentage of elastic energy error to each value of percentage of higher order elastic energy. The coefficients *A* and *B* are solved versus the Poisson´s ratio by

using the mesh averaging of the root-mean-square values Eq. (71) and (72) displayed for the element QU8 in Table 3 and for the element TR6 in Table 4,

$$\begin{aligned}\overline{\varepsilon_1^{RMS}}(\nu) &= [A(\nu) * e_{h1} + B(\nu)] * e_{h1}^2 \\ \overline{\varepsilon_2^{RMS}}(\nu) &= [A(\nu) * e_{h2} + B(\nu)] * e_{h2}^2\end{aligned} \tag{73}$$

By considering Eq. (73) we obtain, for the element QU8 the averaged correlations,

$$\begin{aligned}\varepsilon_P^{QU8} &= [A_P^{QU8}(\nu) * e_h + B_P^{QU8}(\nu)] * e_h^2, \quad 0 < e_h \le 0.20 \\ \varepsilon_S^{QU8} &= [A_S^{QU8}(\nu) * e_h + B_S^{QU8}(\nu)] * e_h^2, \quad 0 < e_h \le 0.20\end{aligned} \tag{74}$$

$$\begin{aligned}\varepsilon_{PL}^{QU8} &= [A_{PL}^{QU8}(\nu) * e_h + B_{PL}^{QU8}(\nu)] * e_h^2, \quad 0 < e_h \le 0.20 \\ \varepsilon_{SH0}^{QU8} &= [A_{SH0}^{QU8}(\nu) * e_h + B_{SH0}^{QU8}(\nu)] * e_h^2, \quad 0 < e_h \le 0.20\end{aligned} \tag{75}$$

Similarly, for the element TR6,

$$\begin{aligned}\varepsilon_P^{TR6} &= [A_P^{TR6}(\nu) * e_h + B_P^{TR6}(\nu)] * e_h^2, \quad 0 < e_h \le 0.09 \\ \varepsilon_S^{TR6} &= [A_S^{TR6}(\nu) * e_h + B_S^{TR6}(\nu)] * e_h^2, \quad 0 < e_h \le 0.09\end{aligned} \tag{76}$$

$$\begin{aligned}\varepsilon_{PL}^{TR6} &= [A_{PL}^{TR6}(\nu) * e_h + B_{PL}^{TR6}(\nu)] * e_h^2, \quad 0 < e_h \le 0.09 \\ \varepsilon_{SH0}^{TR6} &= [A_{SH0}^{TR6}(\nu) * e_h + B_{SH0}^{TR6}(\nu)] * e_h^2, \quad 0 < e_h \le 0.09\end{aligned} \tag{77}$$

It can be observed that the averaged correlations are highly depended on the element considered. In each case the interval of application could be moderately extended beyond the upper limit of percentage of higher order elastic energy used to compute the coefficients *A* and *B*. From Tables 3 and 4, the following inequalities can be deduced,

$$\begin{aligned}\varepsilon_P(e_h, \nu_a) > \varepsilon_S(e_h, \nu_a), \quad 0.05 \le \nu_a \le 0.45 \\ \varepsilon_{PL}(e_h, \nu_a) > \varepsilon_{SH0}(e_h, \nu_a), \quad 0.05 \le \nu_a \le 0.45\end{aligned} \tag{78}$$

$$\begin{aligned}(\varepsilon_P(e_h, \nu_a) - \varepsilon_S(e_h, \nu_a)) < (\varepsilon_P(e_h, \nu_b) - \varepsilon_S(e_h, \nu_b)), \quad 0.05 \le \nu_a < \nu_b \le 0.45 \\ (\varepsilon_{PL}(e_h, \nu_a) - \varepsilon_{SH0}(e_h, \nu_a)) < (\varepsilon_{PL}(e_h, \nu_b) - \varepsilon_{SH0}(e_h, \nu_b)), \quad 0.05 \le \nu_a < \nu_b \le 0.45\end{aligned} \tag{79}$$

Mean values of the second reference value for the indicators of dispersion associated with the phase and group velocities, Eq. (69) and (70), are computed, for each of the test meshes considered and four values of Poisson´s ratio. Mesh averaging of these mean values are displayed for the element QU8 in Table 5 and for the element TR6 in Table 6.

		QU8			
		ν = 0.45	ν = 0.33	ν = 0.25	ν = 0.05
$\overline{e_{p2}^M}$	P	1.00263	1.00280	1.00288	1.00301
	S	1.00947	1.00560	1.00497	1.00433
	PL	1.00282	1.00288	1.00292	1.00301
	SH0	1.00540	1.00496	1.00474	1.00433
$\overline{e_{g2}^M}$	P	1.01268	1.01359	1.01399	1.01465
	S	1.04651	1.02757	1.02444	1.02129
	PL	1.01370	1.01399	1.01418	1.01466
	SH0	1.02657	1.02439	1.02329	1.02127

Table 5: Mesh averaging of the mean values of the second reference value for the indicators of dispersion associated with the phase and group velocities. Element QU8.

		TR6			
		$\nu = 0.45$	$\nu = 0.33$	$\nu = 0.25$	$\nu = 0.05$
$\overline{e_{p2}^{M}}$	P	1.00163	1.00171	1.00175	1.00181
	S	1.00502	1.00306	1.00275	1.00244
	PL	1.00172	1.00175	1.00177	1.00181
	SH0	1.00297	1.00275	1.00264	1.00244
$\overline{e_{g2}^{M}}$	P	1.00775	1.00819	1.00837	1.00867
	S	1.02396	1.01471	1.01322	1.01172
	PL	1.00824	1.00838	1.00846	1.00867
	SH0	1.01423	1.01319	1.01266	1.01171

Table 6: Mesh averaging of the mean values of the second reference value for the indicators of dispersion associated with the phase and group velocities. Element TR6.

2.6 Substitute wave field

It is clear that the harmonic elastic waves cannot be exactly captured by a regular mesh of finite elements QU8 or TR6. This fact is a consequence of the element interpolation which is quadratic. A substitute wave field [19] or alias field [20] has been obtained in the discretized unbounded medium by performing a dispersion analysis in terms of the allowable polarizations of the continuum. The substitute wave field is obtained by collocating Eq. (38) in each node of the unit cell. The assumption of different amplitudes is introduced because the equation of equilibrium is different for each node. The analysis yields the relative wave amplitudes and the dispersion relation under which the alias field may propagate in the discretized medium. The alias wave field will be

$$\widetilde{\mathbf{u}}^{a} = \sum N_{S,i} \widetilde{\mathbf{u}}_{i} \tag{80}$$

where: $\widetilde{\mathbf{u}}_{i}$, the values of Eq. (38) at the nodes; $N_{S,i}$, the nodal shape functions.

2.7 Influence of the Poisson´s ratio

2.7.1 Elastic energy error

For a plane-strain solid and longitudinal waves (P), by considering the Hooke`s law Eq. (5), the denominator in Eq. (2) suggests that significant numerical errors in the stresses could be expected when the Poisson´s ratio approaches the one half value, which can happen for the so-called almost incompressible solids, because the Lamé constant increases indefinitely. The very small volumetric strain, approaching zero in the limit of total incompressibility, is determined from derivatives of displacements, which are not as accurately predicted as the displacements themselves. Any error in the predicted volumetric strain will appear as a large error in the stresses, and this error will in turn significantly increases the elastic energy error. Similarly, for transverse shear waves (S), the alias wave field Eq. (80), which has different amplitude in each node of the unit cell, could produce spurious volumetric strain that also would significantly increase the elastic energy error when the Poisson´s ratio approaches the one half value. This behaviour is the well-known dilatational locking [21, 20], and its effect on elastic energy error is clearly observed in the results displayed in Tables 3 and 4.

For a generalized plane-stress plate, by considering the Hooke`s law Eq. (7), when the Poisson´s ratio approaches the one half value and the Lamé constant increases indefinitely, the constant Eq. (8) also increases but non-indefinitely; therefore, although the elastic energy error

increases when the Poisson´s ratio approaches the one half value, the effect of dilatational locking must not be expected, see Tables 3 and 4.

As conclusion, it is clearly observed that the volumetric strain error must have a prevailing effect on the elastic energy error, increasing the elastic energy error for the longitudinal waves versus the one for the shear waves, Eq. (78). The difference between them is all the greater as the Poisson´s ratio is greater, in accordance with the inequality Eq. (79).

2.7.2 Indicators of dispersion

For a plane-strain solid and P-waves, the system of characteristic equations Eq. (40) is formed by using the dimensionless elasticity matrix Eq. (15). The non-constant components in this matrix are weakly depended on the Poisson´s ratio, Fig. 7. Then, it is expected that the characteristic frequency equation Eq. (45) would be also weakly depended on the Poisson´s ratio and so the dimensionless frequencies computed would be. However, for the S-waves, the system of characteristic equations Eq. (40) is formed by using Eq. (16). The non-constant components in this matrix increase indefinitely when the Poisson´s ratio approaches the one half value, Fig. 7. Then, by considering Eq. (41), it would be expected a significant increase in the computed values of the coefficients associated to the global stiffness matrix and therefore a corresponding increase in the computed values of dimensionless frequency. The effect of this behaviour on the indicators of dispersion Eq. (58) and (59) is clearly observed in the results displayed in Tables 5 and 6. The value of each indicator for the S-waves is greater than the one for the P-waves and the difference between them is all the greater as the Poisson´s ratio is greater, as it would be expected.

Similar arguments can be used for a generalized plane-stress plate. In this case, the dimensionless elasticity matrices Eq. (19) and (20) have non-constant components which are weakly depended on the Poisson´s ratio, Fig. 8; nevertheless, the ones corresponding to the SH0-waves are greater than the ones corresponding to the PL-waves and the difference between them is all the greater as the Poisson´s ratio is greater. The effect of this behaviour is also clearly displayed in Tables 5 and 6.

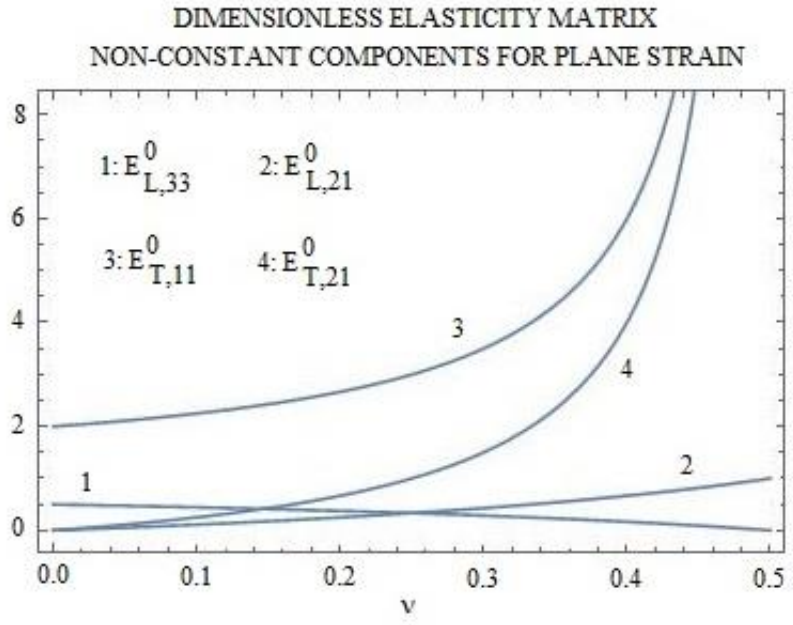

Figure 7: Dimensionless elasticity matrix. Non-constant components for plain strain versus the Poisson´s ratio.

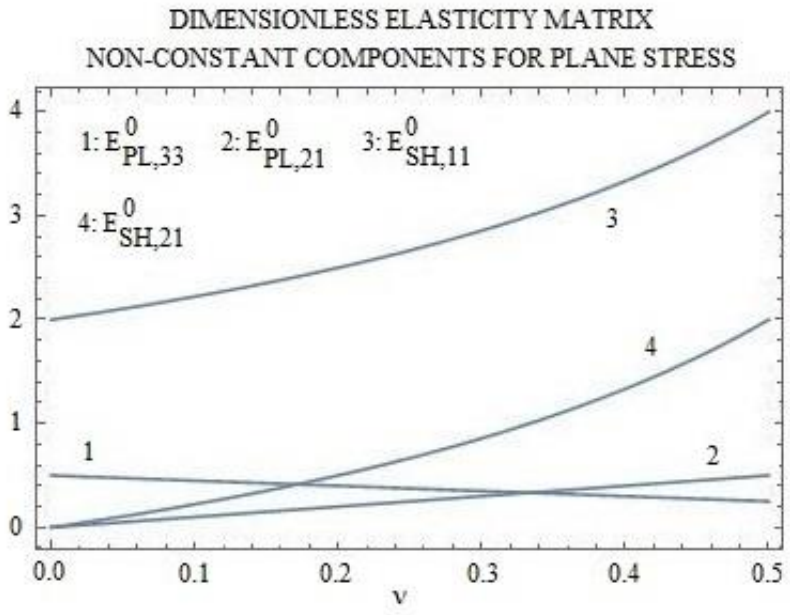

Figure 8: Dimensionless elasticity matrix. Non-constant components for generalized plain stress versus the Poisson´s ratio.

3 MODAL ANALYSIS

3.1 Introduction

By considering the homogeneous part of Eq. (28) and assuming stationary waves, it is yielded the so called generalized eigenproblem [21],

$$(\mathbf{K} - \omega^2 \mathbf{M})\widetilde{\boldsymbol{\psi}} = \mathbf{0} \tag{81}$$

Nontrivial solutions exist only if the determinant of the coefficient matrix is equal to zero,

$$\det(\mathbf{K} - \omega^2 \mathbf{M}) = 0 \tag{82}$$

The above Eq. (82) leads to a polynomial of order n in ω^2 that possesses, in general, n distinct roots. These roots, denoted by

$$\omega_j^2, \quad j = 1, \ldots, n \tag{83}$$

are called eigenvalues. Their square roots are the finite element natural frequencies.

Associated with each eigenvalue Eq. (83) there is an n-dimensional vector whose elements are real numbers. The vector can be obtained by using Eq. (81) as follows,

$$(\mathbf{K} - \omega_j^2 \mathbf{M})\widetilde{\boldsymbol{\psi}}_j = \mathbf{0} \tag{84}$$

where the vector $\widetilde{\boldsymbol{\psi}}_j$ is known as an eigenvector or modal vector.

In this research the generalized eigenproblem has been solved by the subspace iteration method [21]. The eigenvector and the element interpolation functions shape the finite element natural mode. As the finite element mesh is refined and discretization error decreases, both the finite element natural frequencies and the finite element natural modes must converge to the eigenvalues and the eigenfunctions associated with the differential equation of motion and its boundary conditions [22].

An important relation fulfilled by the eigenvectors is that of **M**-orthonormality,

$$\widetilde{\boldsymbol{\psi}}_i^t \mathbf{M} \widetilde{\boldsymbol{\psi}}_j = \delta_{ij} \tag{85}$$

where: δ_{ij}, Kronecker delta.

Premultiplying Eq. (84) by $\widetilde{\boldsymbol{\psi}}_i^t$ and using Eq. (85), it is yielded

$$\widetilde{\boldsymbol{\psi}}_i^T \mathbf{K} \widetilde{\boldsymbol{\psi}}_j = \delta_{ij} \omega_j^2 \tag{86}$$

Finally, by introducing Eq. (86) into Eq. (34), the following expression for the modal elastic energy is yielded

$$\overline{E}_j = \tfrac{1}{4} \omega_j^2, \quad j = 1, \ldots, n \tag{87}$$

3.2 Numerical research

In this section the application of the percentage of higher order elastic energy as an error indicator for the natural modes computed by the finite element method is investigated. This percentage will be evaluated by Eq. (34) and (35). An estimation of the error for the modal elastic energies obtained with the discretized elastic domain will be presented. The reference model will be produced by dividing each element of the actual mesh into sixteen elements. The elastic energies obtained with the actual model and the ones obtained with the reference model will be compared by the modal elastic energy error

$$EEE = (\overline{E} / \overline{E}^{REF}) - 1 \tag{88}$$

where $\overline{E}$ and $\overline{E}^{REF}$ are defined by Eq. (34). By considering Eq. (87), the modal elastic energy error Eq. (88) can be evaluated as

$$EEE = (\omega / \omega^{REF})^2 - 1 \tag{89}$$

In order to investigate the behaviour of the higher order elastic energy as a modal error indicator, the application of the averaged correlations, Eq. (74) - (77), yielded by the numerical dispersion analysis, between the percentage of higher order elastic energy and the elastic energy error is explored. For a plane-strain solid, the elastic energy error estimated by the P and S averaged correlations, Eq. (74) for QU8 element and Eq. (76) for TR6 element, from the percentage of higher order modal elastic energy computed with the actual model, will be called the standard elastic energy error based on the P and S waves, $SEEE_P$ and $SEEE_S$, respectively. Similarly, for a generalized plane-stress plate, the elastic energy error estimated by the PL and SH0 averaged correlations, Eq. (75) for QU8 element and Eq. (77) for TR6 element, will be called the standard elastic energy error based on the PL and SH0 waves, $SEEE_{PL}$ and $SEEE_{SH0}$, respectively. By considering Eq. (78), the standard modal elastic energy error is defined as,

$$\begin{aligned} SEEE(PHE, \nu) &= \tfrac{1}{2}(SEEE_P + SEEE_S) \\ SEEE(PHE, \nu) &= \tfrac{1}{2}(SEEE_{PL} + SEEE_{SH0}) \end{aligned} \tag{90}$$

where: *PHE*, percentage of higher order elastic energy computed with the actual model.

From Tables 3 and 4, the inequality $SEEE(PHE, \nu_a) < SEEE(PHE, \nu_b)$ can be deduced; where: $0.05 \le \nu_a < \nu_b \le 0.45$.

In order to compare the standard modal elastic energy error Eq. (90) with the modal elastic energy error Eq. (89), two typical plane-strain solids will be analyzed: earth dam discretized by a regular mesh of TR6 elements [23], Fig. 9; and bridge pier discretized by a quasi-regular mesh of QU8 elements [24], Fig. 11. Similarly, two typical generalized plane-stress plates will be

analyzed: cantilever shear wall discretized by a regular mesh of QU8 elements [23], Fig. 13; and Cook's membrane discretized by a quasi-regular mesh of TR6 elements [25], Fig. 15. For the last one three different materials with increasing Poisson´s ratio are considered. It must be remarked that if the structure considered has an axis of symmetry, the modes can be obtained by idealizing a half of it and applying two combinations of boundary conditions on the axis for symmetric motion (S) and for antisymmetric motion (A), see reference [23]. The results of the analysis are displayed in Fig. 10, 12, 14 and 16 and Tables 7-10.

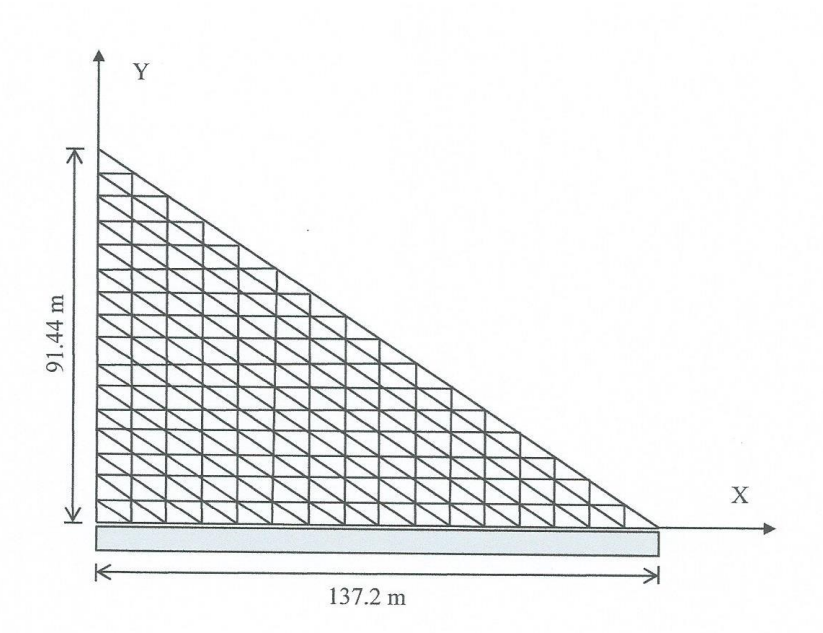

Figure 9: Half of earth dam. E = 5.605 x 10^8 Pa, ν = 0.45, ρ = 2082 kg/m^3.

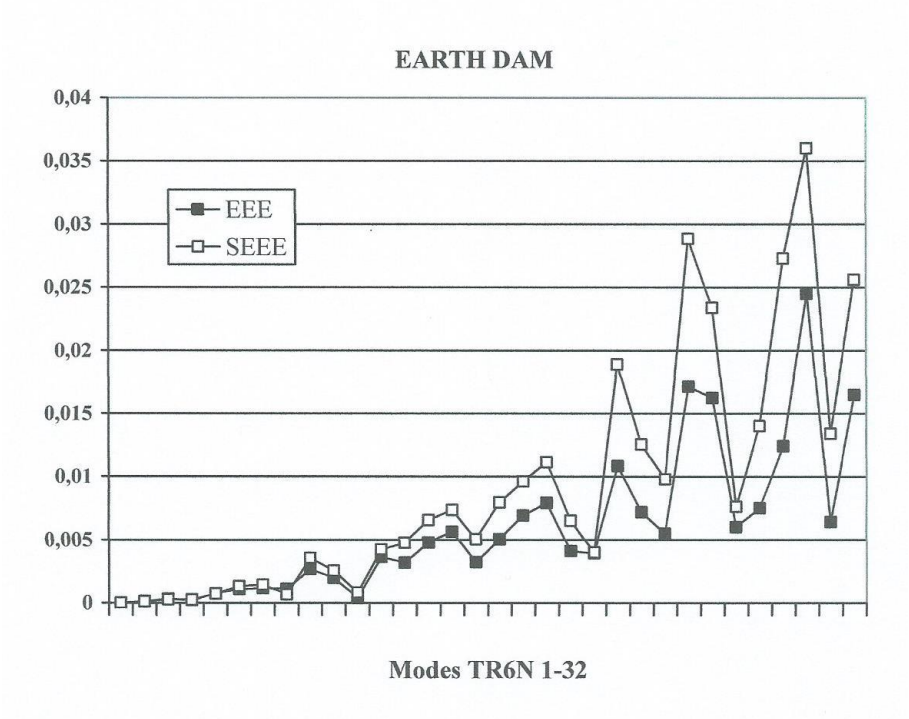

Figure 10: Earth dam. Standard modal elastic energy error SEEE versus modal elastic energy error computed by mesh halving EEE. Modes 1-32.

MODES		FR (Hz)	PHE	EEE	SEEE	PHE REF
1	A	1.236	0.000522	0.000008	0.000001	0.000034
2	S	1.987	0.005229	0.000126	0.000091	0.000325
3	A	2.296	0.008874	0.000300	0.000262	0.000550
4	A	2.919	0.008593	0.000209	0.000246	0.000537
5	S	3.215	0.014675	0.000745	0.000720	0.000914
6	S	3.567	0.019746	0.001061	0.001307	0.001218
7	A	3.652	0.020730	0.001144	0.001442	0.001295
8	S	4.222	0.014035	0.001106	0.000658	0.000873
9	A	4.234	0.032380	0.002656	0.003542	0.001995
10	S	4.486	0.027416	0.001973	0.002532	0.001726
11	A	4.540	0.015450	0.000388	0.000798	0.000971
12	S	4.980	0.035384	0.003624	0.004237	0.002199
13	A	5.145	0.037475	0.003180	0.004759	0.002790
14	A	5.160	0.043888	0.004773	0.006552	0.002304
15	S	5.533	0.046500	0.005650	0.007367	0.002875
16	S	5.797	0.038594	0.003234	0.005051	0.002473
17	A	6.034	0.048296	0.005038	0.007955	0.003335
18	S	6.069	0.052987	0.006918	0.009602	0.003337
19	A	6.134	0.056985	0.007917	0.011133	0.003263
20	A	6.415	0.043759	0.004117	0.006513	0.002828
21	A	6.579	0.034377	0.003938	0.003997	0.002249
22	S	6.626	0.073854	0.010825	0.018886	0.004621
23	S	7.028	0.060433	0.007187	0.012546	0.003974
24	A	7.055	0.053462	0.005491	0.009778	0.003429
25	A	7.127	0.090799	0.017119	0.028830	0.005561
26	S	7.222	0.081937	0.016236	0.023356	0.005218
27	S	7.604	0.047281	0.006021	0.007620	0.003035
28	A	7.715	0.063779	0.007508	0.014001	0.004258
29	S	7.723	0.088368	0.012415	0.027268	0.005671
30	A	7.899	0.101168	0.024466	0.036006	0.007130
31	A	8.039	0.062396	0.006408	0.013390	0.003321
32	S	8.194	0.085678	0.016472	0.025593	0.005629

FR, natural frequency computed with the actual model; PHE, percentage of higher order elastic energy computed with the actual model; EEE, elastic energy error computed by mesh halving; SEEE, standard elastic energy error; PHE REF, percentage of higher order elastic energy computed by mesh halving.

Table 7: Earth dam. Estimation of the discretization error. Modes 1-32.

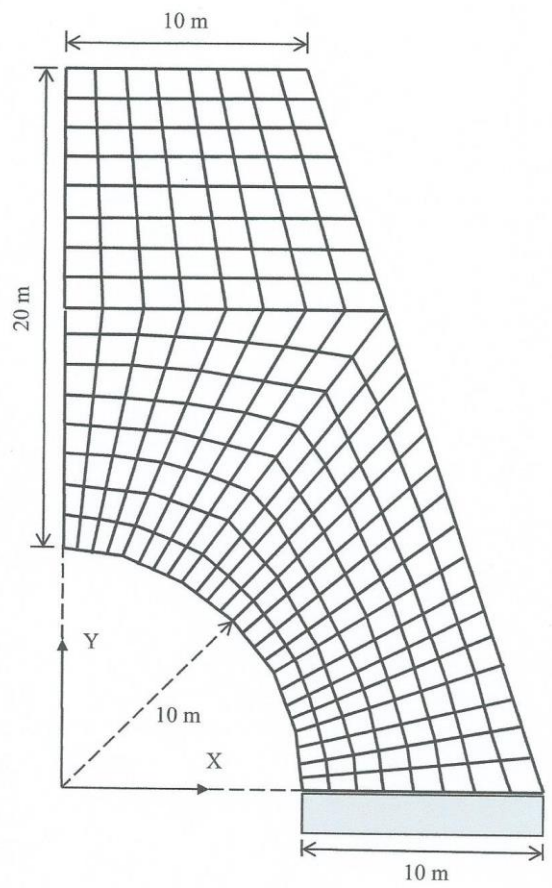

Figure 11: Half of bridge pier. E = 40 x 10^9 Pa, ν = 0.15, ρ = 2400 kg/m^3.

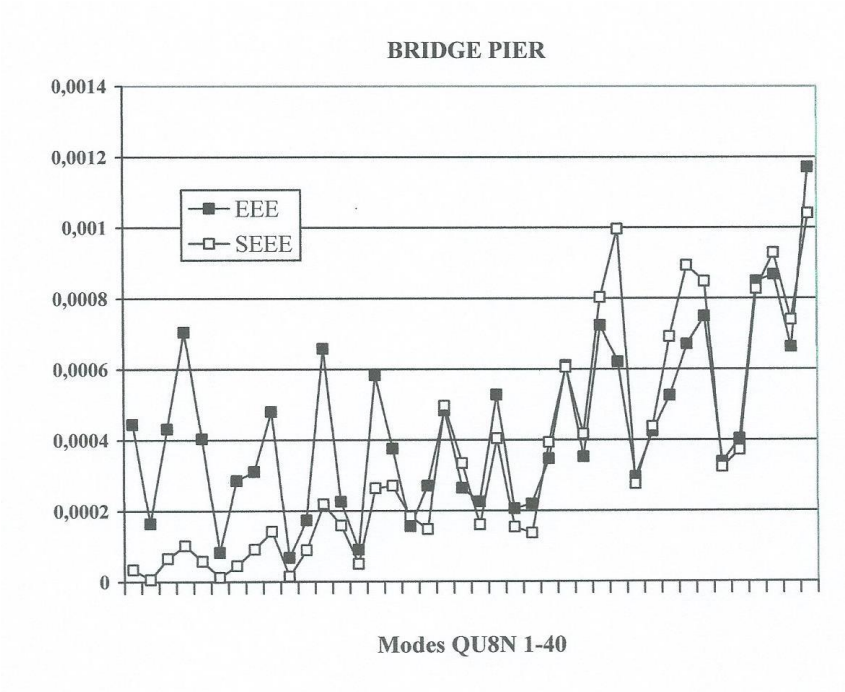

Figure 12: Bridge pier. Standard modal elastic energy error SEEE versus modal elastic energy error computed by mesh halving EEE. Modes 1-40.

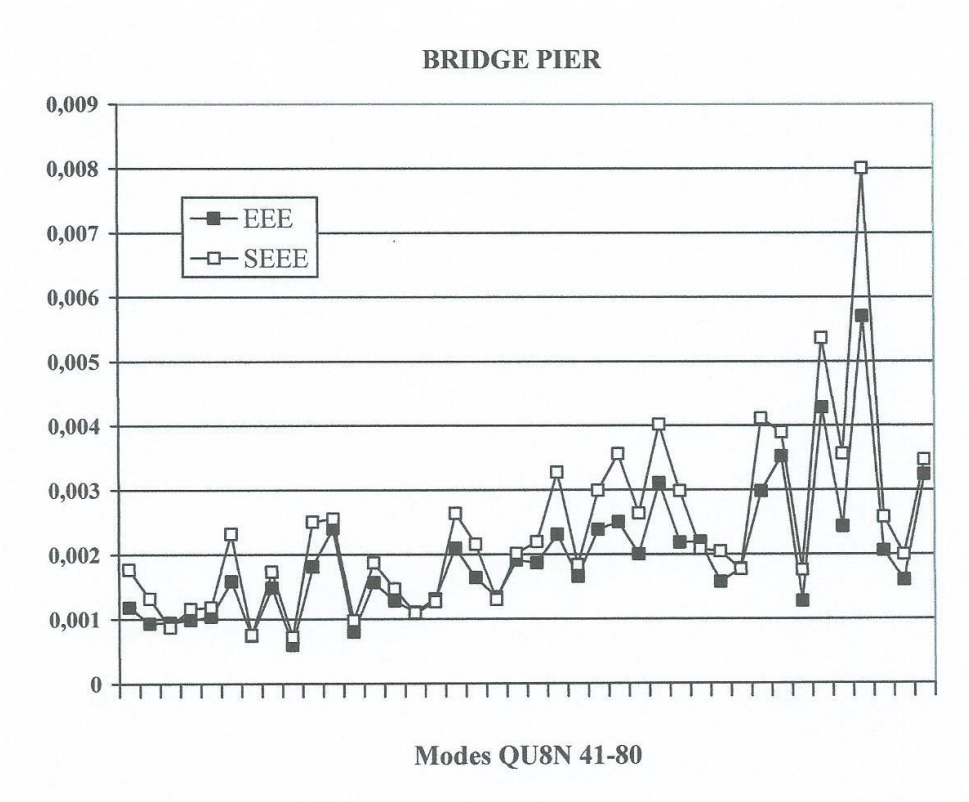

Figure 12 (cont.): Bridge pier. Standard modal elastic energy error SEEE versus modal elastic energy error computed by mesh halving EEE. Modes 41-80.

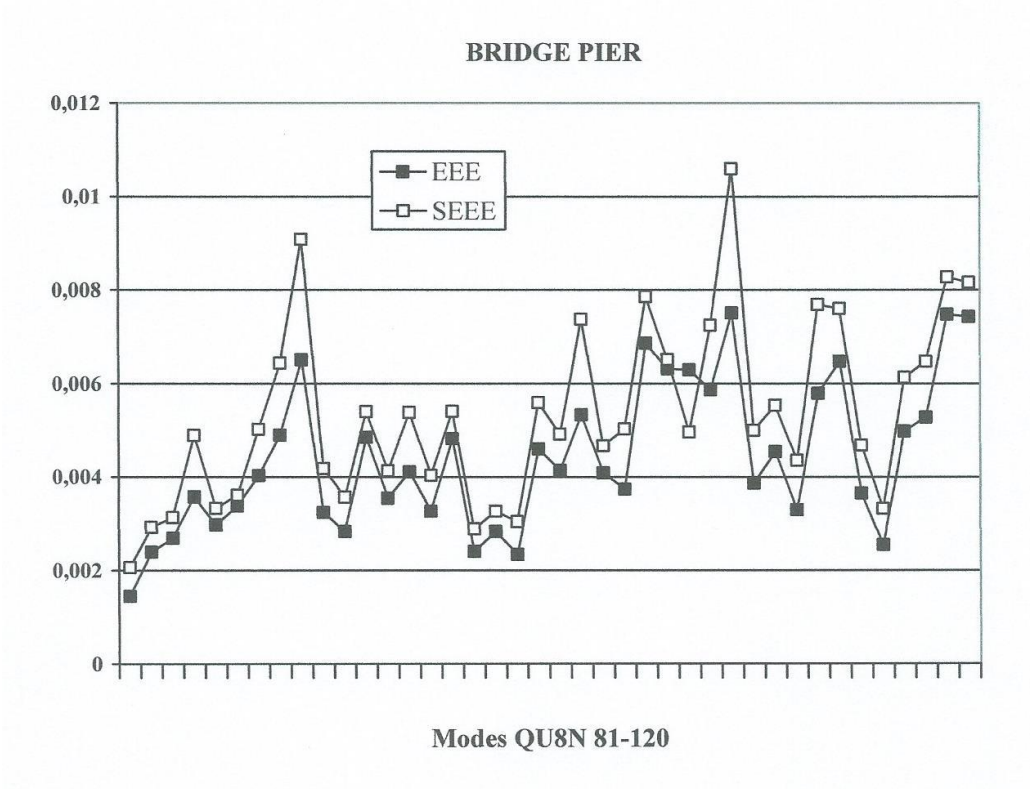

Figure 12 (cont.): Bridge pier. Standard modal elastic energy error SEEE versus modal elastic energy error computed by mesh halving EEE. Modes 81-120.

MODES		FR (Hz)	PHE	EEE	SEEE	PHE REF
1	A	15.90	0.010837	0.000444	0.000034	0.000907
2	S	26.79	0.004623	0.000164	0.000006	0.000386
3	A	31.97	0.014868	0.000431	0.000065	0.001137
4	S	58.86	0.018576	0.000705	0.000101	0.001512
5	A	71.57	0.014031	0.000403	0.000058	0.001089
6	S	79.38	0.006482	0.000082	0.000012	0.000443
7	A	87.13	0.012466	0.000285	0.000045	0.000912
8	S	89.69	0.017574	0.000311	0.000091	0.001259
9	A	103.25	0.021950	0.000480	0.000142	0.001629
10	S	104.14	0.007174	0.000067	0.000015	0.000479
11	S	117.92	0.017451	0.000174	0.000089	0.001177
12	S	123.66	0.027234	0.000658	0.000219	0.002056
13	A	127.24	0.023259	0.000226	0.000159	0.001554
14	A	138.92	0.013091	0.000090	0.000050	0.000860
15	A	143.06	0.029835	0.000583	0.000264	0.002170
16	S	153.20	0.030231	0.000375	0.000271	0.002057
17	A	156.29	0.024988	0.000156	0.000184	0.001613
18	S	165.68	0.022446	0.000271	0.000148	0.001542
19	A	165.84	0.040767	0.000483	0.000497	0.002771
20	S	170.64	0.033507	0.000265	0.000334	0.002220
21	A	178.14	0.023398	0.000226	0.000161	0.001572
22	S	182.11	0.036819	0.000528	0.000404	0.002537
23	A	186.98	0.022837	0.000206	0.000154	0.001515
24	S	193.49	0.021542	0.000220	0.000137	0.001460
25	A	195.09	0.036313	0.000347	0.000393	0.002406
26	S	202.48	0.044920	0.000611	0.000605	0.003062
27	A	202.73	0.037403	0.000352	0.000417	0.002487
28	A	207.97	0.051592	0.000724	0.000803	0.003539
29	S	210.07	0.057312	0.000621	0.000996	0.003809
30	S	216.87	0.030490	0.000296	0.000276	0.002025
31	A	223.79	0.038330	0.000425	0.000438	0.002532
32	S	228.36	0.047980	0.000526	0.000692	0.003216
33	S	230.11	0.054366	0.000671	0.000894	0.003641
34	A	231.49	0.052977	0.000750	0.000848	0.003693
35	A	234.27	0.033038	0.000338	0.000324	0.002205
36	S	240.06	0.035344	0.000403	0.000372	0.002362
37	A	246.31	0.052356	0.000848	0.000827	0.003673
38	S	247.35	0.055403	0.000867	0.000929	0.003806
39	A	247.53	0.049585	0.000663	0.000740	0.003293
40	S	253.31	0.058542	0.001171	0.001040	0.004264

Table 8: Bridge pier. Estimation of the discretization error. Modes 1-40.

MODES		FR (Hz)	PHE	EEE	SEEE	PHE REF
41	A	256.32	0.075797	0.001182	0.001768	0.005140
42	S	259.43	0.065695	0.000929	0.001317	0.004436
43	A	261.03	0.053658	0.000945	0.000870	0.003698
44	S	268.43	0.061682	0.000984	0.001157	0.004208
45	A	273.92	0.062382	0.001040	0.001184	0.004379
46	A	279.51	0.086516	0.001586	0.002323	0.005983
47	S	280.79	0.049903	0.000737	0.000750	0.003359
48	A	282.72	0.075127	0.001488	0.001736	0.005262
49	S	285.94	0.048788	0.000601	0.000716	0.003290
50	A	287.63	0.089749	0.001817	0.002507	0.006156
51	S	288.84	0.090531	0.002408	0.002552	0.006642
52	A	296.41	0.056752	0.000797	0.000976	0.003902
53	S	296.85	0.077968	0.001567	0.001874	0.005517
54	S	307.96	0.069279	0.001281	0.001469	0.004831
55	A	308.60	0.059947	0.001109	0.001092	0.004281
56	S	308.72	0.064432	0.001313	0.001266	0.004407
57	A	309.55	0.092001	0.002101	0.002639	0.006432
58	S	315.10	0.083578	0.001643	0.002163	0.005739
59	A	319.48	0.065320	0.001342	0.001302	0.004656
60	S	322.94	0.080844	0.001911	0.002019	0.005744
61	A	324.53	0.084293	0.001870	0.002201	0.005912
62	S	325.84	0.102075	0.002313	0.003274	0.007330
63	A	327.00	0.077302	0.001661	0.001841	0.005488
64	A	328.46	0.097755	0.002390	0.002993	0.006740
65	S	331.48	0.106303	0.002502	0.003563	0.007333
66	S	338.27	0.091968	0.002006	0.002637	0.006313
67	A	343.64	0.112611	0.003110	0.004019	0.008251
68	S	347.44	0.097600	0.002185	0.002983	0.006727
69	S	350.85	0.082148	0.002201	0.002087	0.006124
70	A	350.88	0.081406	0.001575	0.002048	0.005610
71	A	353.01	0.075778	0.001781	0.001767	0.005178
72	A	357.34	0.113835	0.002982	0.004111	0.008200
73	S	359.73	0.110938	0.003525	0.003895	0.008354
74	S	360.63	0.075589	0.001275	0.001758	0.005032
75	S	365.72	0.129216	0.004282	0.005360	0.009435
76	A	366.02	0.106311	0.002435	0.003564	0.007359
77	A	371.50	0.156259	0.005698	0.008004	0.011536
78	S	373.36	0.091041	0.002060	0.002582	0.006362
79	A	375.69	0.080482	0.001598	0.002001	0.005408
80	S	379.47	0.104977	0.003241	0.003471	0.007850

Table 8 (cont.): Bridge pier. Estimation of the discretization error. Modes 41-80.

MODES		FR (Hz)	PHE	EEE	SEEE	PHE REF
81	S	382.50	0.081658	0.001445	0.002062	0.005477
82	A	382.53	0.096618	0.002396	0.002921	0.006797
83	A	385.63	0.099907	0.002690	0.003131	0.007215
84	S	393.14	0.123699	0.003575	0.004891	0.008919
85	A	393.25	0.102855	0.002975	0.003327	0.007503
86	S	396.98	0.106919	0.003378	0.003606	0.007597
87	A	397.37	0.125210	0.004025	0.005018	0.009328
88	S	398.99	0.140966	0.004900	0.006438	0.010554
89	A	401.79	0.165861	0.006509	0.009084	0.012033
90	A	403.46	0.114698	0.003241	0.004176	0.007852
91	A	406.39	0.106358	0.002837	0.003567	0.007987
92	S	407.04	0.129658	0.004849	0.005399	0.009640
93	A	412.99	0.114120	0.003545	0.004132	0.008322
94	S	413.48	0.129431	0.004107	0.005379	0.009198
94	A	415.48	0.112774	0.003263	0.004031	0.007617
96	S	418.33	0.129725	0.004815	0.005405	0.009135
97	S	421.58	0.096085	0.002404	0.002888	0.006860
98	A	421.82	0.101983	0.002833	0.003268	0.007309
99	S	425.41	0.098569	0.002341	0.003045	0.006759
100	A	429.42	0.131821	0.004598	0.005590	0.010021
101	S	431.38	0.124019	0.004139	0.004918	0.009206
102	A	433.42	0.150311	0.005326	0.007373	0.010895
103	S	433.90	0.120922	0.004086	0.004664	0.009141
104	A	436.98	0.125299	0.003735	0.005025	0.009075
105	S	440.02	0.154896	0.006865	0.007857	0.012240
106	S	444.36	0.141772	0.006312	0.006516	0.012018
107	A	445.10	0.124530	0.006295	0.004961	0.011756
108	A	447.10	0.149073	0.005863	0.007245	0.008758
109	S	448.03	0.178314	0.007507	0.010598	0.013018
110	A	449.54	0.124954	0.003863	0.004996	0.008696
111	S	450.78	0.131171	0.004538	0.005532	0.008227
112	S	454.78	0.116980	0.003294	0.004351	0.008650
113	S	455.72	0.153316	0.005787	0.007688	0.010786
114	A	458.28	0.152491	0.006474	0.007601	0.011373
115	A	459.37	0.121113	0.003647	0.004680	0.008535
116	S	460.91	0.102839	0.002545	0.003326	0.007128
117	A	464.75	0.137726	0.004978	0.006130	0.009959
118	A	468.41	0.141359	0.005276	0.006476	0.010834
119	A	470.14	0.158750	0.007480	0.008277	0.012185
120	S	471.41	0.157682	0.007425	0.008159	0.012499

Table 8 (cont.): Bridge pier. Estimation of the discretization error. Modes 81-120.

MODES		FR (Hz)	PHE	EEE	SEEE	PHE REF
121	A	471.99	0.147194	0.004995	0.007053	0.010705
122	S	475.53	0.162324	0.007614	0.008677	0.013276
123	S	478.27	0.173088	0.007153	0.009947	0.012727
124	A	478.91	0.141254	0.005976	0.006466	0.011403
125	S	481.62	0.134171	0.004815	0.005802	0.009893
126	A	482.86	0.134865	0.004648	0.005865	0.009279
127	S	486.12	0.189325	0.010243	0.012046	0.013706
128	S	489.39	0.161129	0.006820	0.008542	0.011256
129	A	490.24	0.198109	0.011994	0.013276	0.015791
130	S	495.44	0.156066	0.006742	0.007983	0.011583
131	A	495.94	0.170228	0.007359	0.009600	0.012443
132	A	497.88	0.198882	0.009871	0.013387	0.015155
133	A	500.63	0.144811	0.004780	0.006814	0.010319
134	S	501.41	0.139267	0.005998	0.006276	0.012044
135	S	504.52	0.147970	0.006089	0.007132	0.010935
136	A	504.84	0.139496	0.005258	0.006297	0.009942
137	S	506.13	0.140117	0.005130	0.006357	0.009497
138	S	510.84	0.163425	0.007258	0.008803	0.012394
139	A	511.43	0.168684	0.007860	0.009416	0.012466
140	S	513.40	0.156476	0.007052	0.008028	0.012980
141	A	513.60	0.139320	0.007587	0.006281	0.015332
142	S	516.32	0.156590	0.007814	0.008040	0.012855
143	A	517.33	0.205883	0.012867	0.014420	0.014351
144	S	522.04	0.204970	0.015769	0.014283	0.017524
145	S	522.38	0.158432	0.005432	0.008242	0.009347
146	A	524.82	0.173084	0.007459	0.009946	0.012496
147	A	525.99	0.251001	0.015592	0.022143	0.018187
148	A	531.82	0.161474	0.006423	0.008581	0.011914
149	S	532.10	0.166622	0.008715	0.009173	0.012792
150	A	534.70	0.203808	0.011586	0.014110	0.015515
151	S	535.09	0.174208	0.008323	0.010084	0.012926
152	A	536.99	0.150662	0.005027	0.007409	0.010646
153	S	540.90	0.164760	0.006852	0.008956	0.012130
154	A	541.19	0.199098	0.010438	0.013418	0.015391
155	A	541.97	0.168369	0.008068	0.009378	0.014395
156	S	542.46	0.208654	0.010853	0.014841	0.016268
157	A	546.24	0.199718	0.011177	0.013508	0.015135
158	S	546.51	0.204861	0.013632	0.014267	0.016700
159	S	549.88	0.196675	0.009864	0.013070	0.014015
160	A	553.20	0.169609	0.007966	0.009526	0.012789

Table 8 (cont.): Bridge pier. Estimation of the discretization error. Modes 121-160.

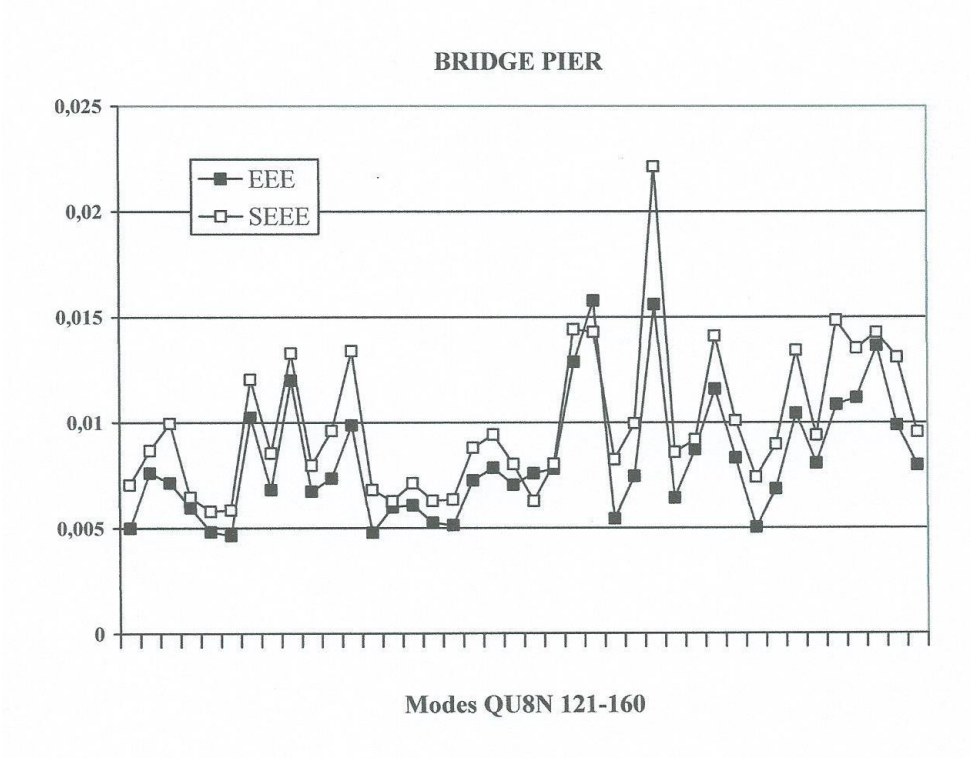

Figure 12 (cont.): Bridge pier. Standard modal elastic energy error SEEE versus modal elastic energy error computed by mesh halving EEE. Modes 121-160.

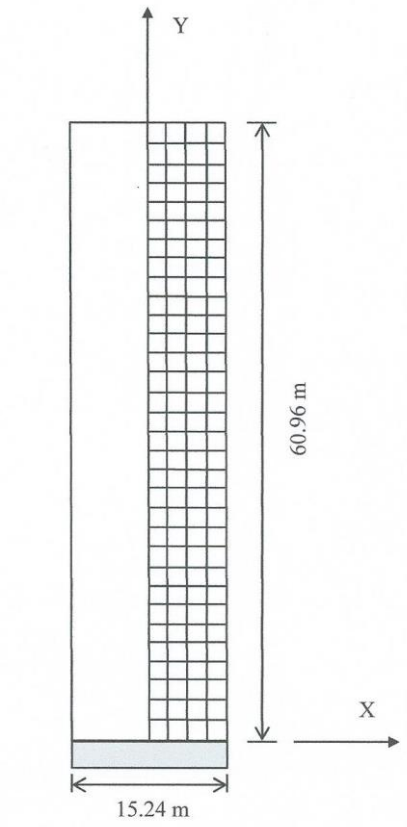

Figure 13: Cantilever shear wall. E = 34.474 x 10^9 Pa, ν = 0.11, ρ = 568.7 kg/m^3.

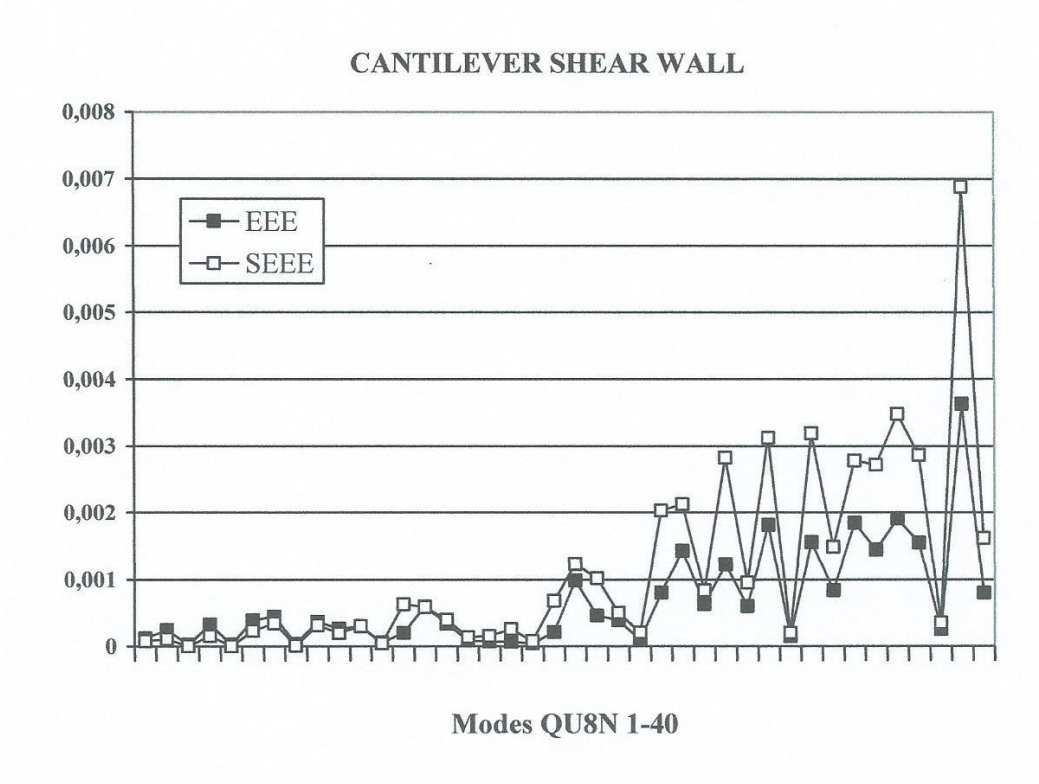

Figure 14: Cantilever shear wall. Standard modal elastic energy error SEEE versus modal elastic energy error computed by mesh halving EEE. Modes 1-40.

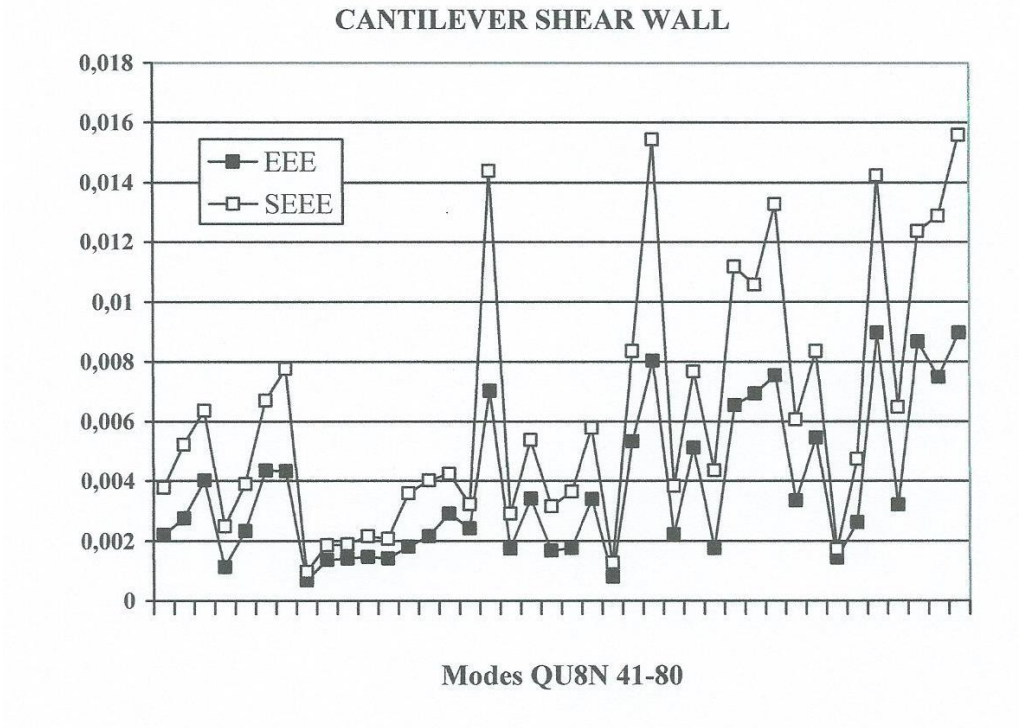

Figure 14 (cont.): Cantilever shear wall. Standard modal elastic energy error SEEE versus modal elastic energy error computed by mesh halving EEE. Modes 41-80.

MODES		FR (Hz)	PHE	EEE	SEEE	PHE REF
1	A	4.95	0.016453	0.000119	0.000078	0.001069
2	A	25.57	0.019286	0.000245	0.000107	0.001292
3	S	31.94	0.000299	0.000023	0.000000	0.000027
4	A	59.33	0.023144	0.000328	0.000155	0.001568
5	S	95.76	0.001919	0.000025	0.000001	0.000129
6	A	96.52	0.028309	0.000390	0.000233	0.001918
7	A	135.26	0.034517	0.000449	0.000348	0.002333
8	S	159.28	0.005231	0.000033	0.000008	0.000338
9	A	169.37	0.033092	0.000369	0.000319	0.002214
10	A	189.08	0.026014	0.000267	0.000196	0.001724
11	A	202.25	0.032400	0.000301	0.000306	0.002145
12	S	220.64	0.012188	0.000056	0.000043	0.000780
13	S	227.22	0.046326	0.000203	0.000632	0.002971
14	A	229.69	0.044709	0.000599	0.000588	0.003024
15	A	242.37	0.037004	0.000342	0.000400	0.002448
16	S	250.38	0.021847	0.000085	0.000138	0.001389
17	S	252.05	0.023033	0.000071	0.000153	0.001462
18	S	253.12	0.029681	0.000068	0.000256	0.001888
19	S	257.03	0.016589	0.000042	0.000079	0.001049
20	S	267.95	0.048140	0.000214	0.000683	0.003120
21	A	272.49	0.064224	0.000987	0.001230	0.004390
22	S	286.47	0.058593	0.000461	0.001020	0.003887
23	A	287.22	0.041427	0.000391	0.000503	0.002746
24	S	292.82	0.026739	0.000098	0.000207	0.001709
25	S	311.13	0.081948	0.000805	0.002029	0.005508
26	A	313.75	0.083797	0.001428	0.002124	0.005773
27	A	334.91	0.053250	0.000631	0.000839	0.003596
28	S	337.51	0.096197	0.001226	0.002824	0.006576
29	S	351.16	0.056683	0.000602	0.000953	0.003711
30	A	352.98	0.100982	0.001816	0.003123	0.006974
31	S	354.48	0.026471	0.000149	0.000203	0.001690
32	S	368.40	0.102029	0.001559	0.003190	0.007056
33	S	375.34	0.070461	0.000837	0.001487	0.004700
34	A	381.64	0.095510	0.001847	0.002783	0.006816
35	A	390.37	0.094463	0.001446	0.002720	0.006314
36	S	400.59	0.106367	0.001908	0.003478	0.007472
37	S	407.75	0.096851	0.001549	0.002864	0.006663
38	S	418.09	0.034715	0.000252	0.000352	0.002221
39	A	418.84	0.147473	0.003632	0.006881	0.010560
40	A	431.06	0.073379	0.000799	0.001616	0.004930

Table 9: Cantilever shear wall. Estimation of the discretization error. Modes 1-40.

MODES		FR (Hz)	PHE	EEE	SEEE	PHE REF
41	S	435.04	0.110661	0.002208	0.003776	0.007832
42	S	443.64	0.129303	0.002753	0.005224	0.009203
43	A	450.18	0.142036	0.004020	0.006359	0.010283
44	A	469.66	0.090482	0.001141	0.002488	0.006179
45	S	471.24	0.112396	0.002336	0.003900	0.007930
46	A	478.40	0.145618	0.004355	0.006700	0.010606
47	S	479.99	0.156249	0.004332	0.007771	0.011945
48	S	482.05	0.057228	0.000684	0.000972	0.003343
49	A	485.27	0.078590	0.001373	0.001861	0.005206
50	A	486.37	0.079230	0.001417	0.001893	0.005255
51	A	493.13	0.084404	0.001477	0.002156	0.005651
52	A	498.37	0.082840	0.001415	0.002074	0.005498
53	A	500.17	0.107927	0.001814	0.003585	0.007460
54	S	508.48	0.114092	0.002161	0.004024	0.007895
55	A	508.65	0.116994	0.002908	0.004240	0.009037
56	A	511.35	0.102418	0.002423	0.003216	0.006821
57	S	516.34	0.208884	0.007029	0.014391	0.015839
58	A	518.54	0.097682	0.001745	0.002915	0.006412
59	A	529.26	0.131089	0.003410	0.005376	0.009266
60	A	534.36	0.101436	0.001674	0.003152	0.006786
61	A	542.45	0.108857	0.001760	0.003649	0.007552
62	S	544.77	0.135741	0.003392	0.005783	0.010938
63	S	545.74	0.065243	0.000805	0.001270	0.003980
64	A	547.24	0.161771	0.005333	0.008362	0.012231
65	S	552.98	0.215835	0.008042	0.015435	0.015606
66	A	561.40	0.111529	0.002217	0.003838	0.007523
67	A	565.74	0.155359	0.005118	0.007678	0.011218
68	A	572.35	0.118540	0.001756	0.004357	0.008030
69	S	579.64	0.185596	0.006544	0.011185	0.015404
70	A	586.98	0.180757	0.006933	0.010575	0.014955
71	S	590.86	0.201136	0.007546	0.013274	0.013963
72	A	591.77	0.138911	0.003342	0.006069	0.009176
73	A	599.76	0.161746	0.005454	0.008359	0.011603
74	S	609.07	0.075817	0.001435	0.001729	0.005808
75	A	612.19	0.123412	0.002627	0.004739	0.008479
76	S	614.19	0.207827	0.008968	0.014236	0.016762
77	A	623.28	0.143350	0.003206	0.006483	0.010250
78	A	627.37	0.194610	0.008666	0.012373	0.017569
79	S	628.04	0.198350	0.007487	0.012885	0.013861
80	A	632.74	0.216859	0.008971	0.015592	0.014049

Table 9 (cont.): Cantilever shear wall. Estimation of the discretization error. Modes 41-80.

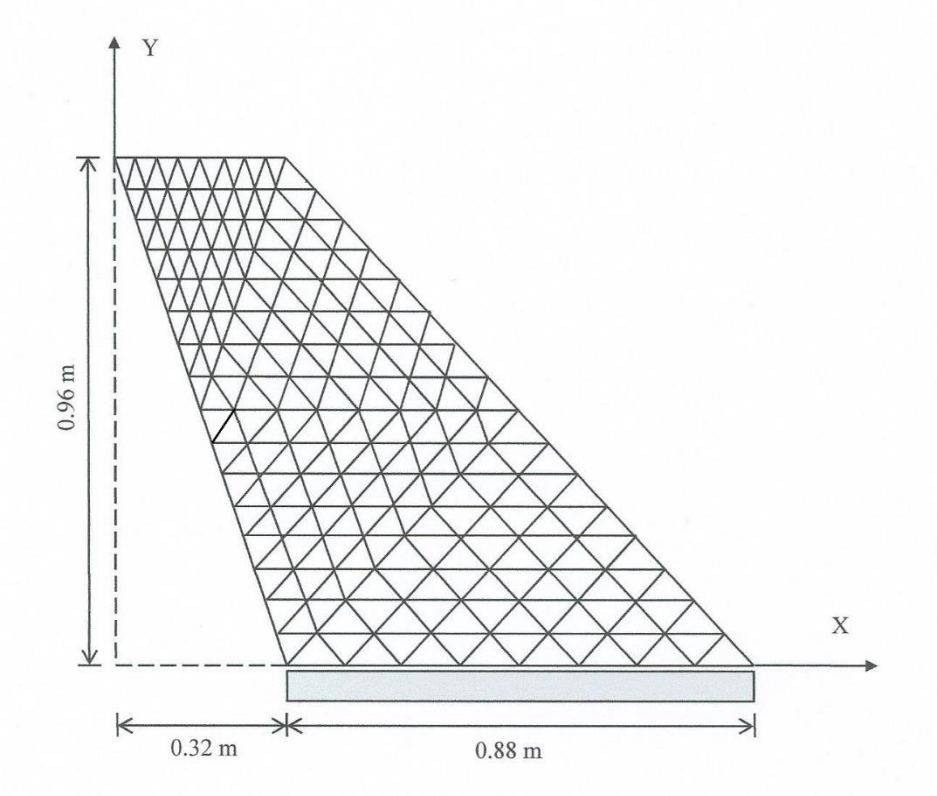

Figure 15: Cook's membrane.

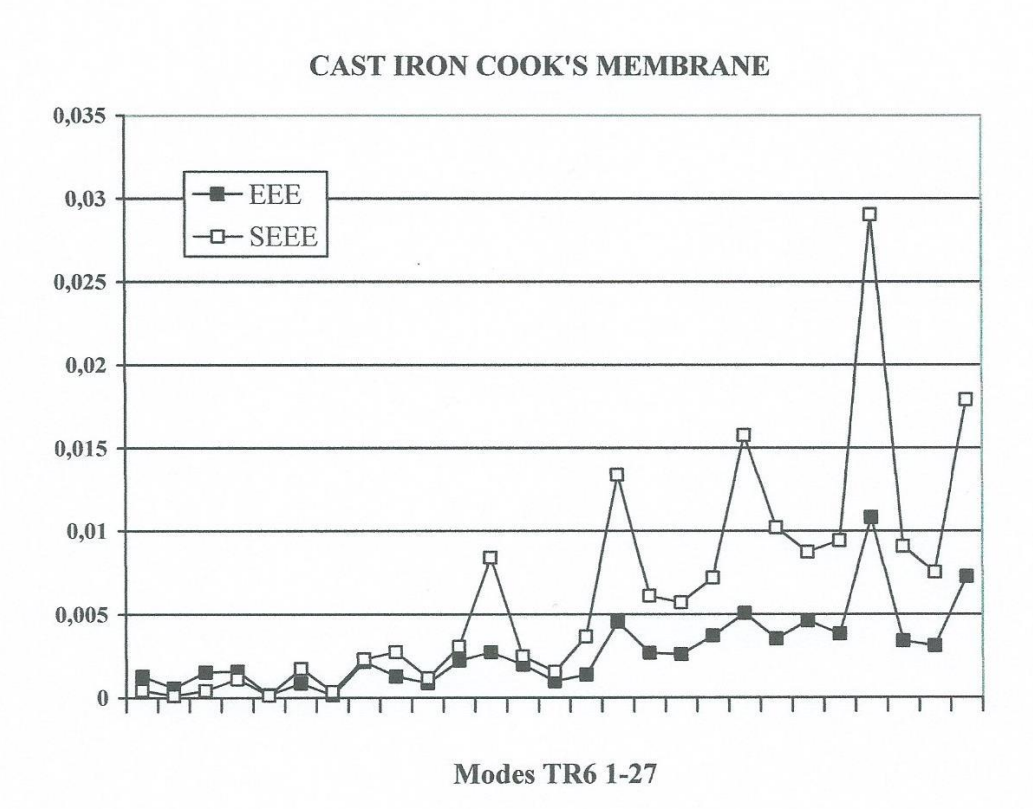

Figure 16: Cast iron Cook's membrane. E = 97 x 10^9 Pa, ν = 0.22, ρ = 7850 kg/m^3. Standard modal elastic energy error SEEE versus modal elastic energy error computed by mesh halving EEE. Modes 1-27.

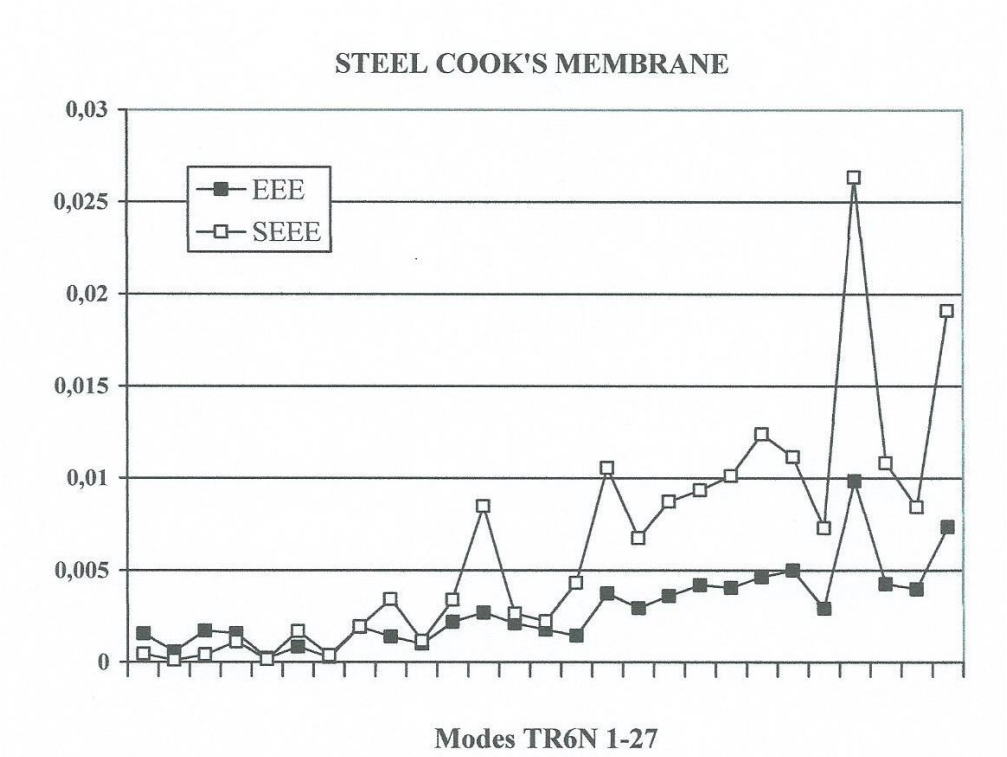

Figure 16 (cont.): Steel Cook's membrane. E = 206.8 x 10^9 Pa, ν = 0.30, ρ = 8058 kg/m^3. Standard modal elastic energy error SEEE versus modal elastic energy error computed by mesh halving EEE. Modes 1-27.

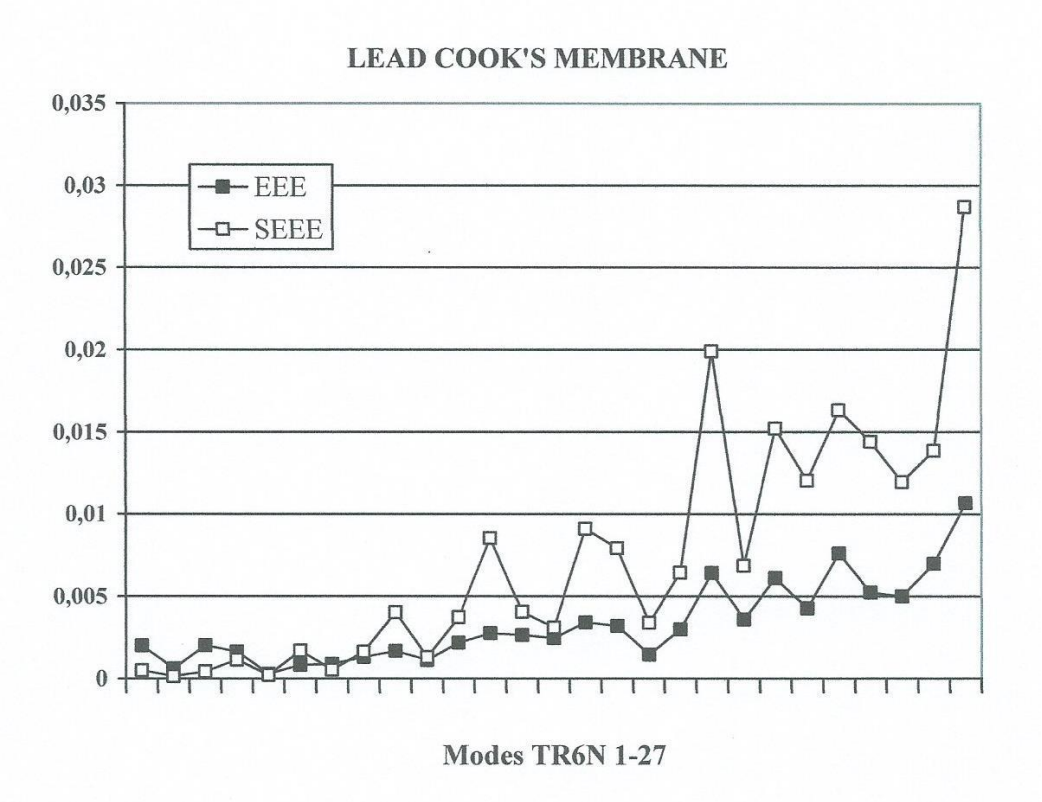

Figure 16 (cont.): Lead Cook's membrane. E = 17 x 10^9 Pa, ν = 0.40, ρ = 11370 kg/m^3. Standard modal elastic energy error SEEE versus modal elastic energy error computed by mesh halving EEE. Modes 1-27.

MODES	FR (Hz)	PHE	EEE	SEEE	PHE REF
1	346.132	0.013745	0.001259	0.000437	0.001247
2	909.875	0.006499	0.000566	0.000097	0.000569
3	1062.797	0.013451	0.001515	0.000418	0.001283
4	1845.525	0.021820	0.001565	0.001107	0.001760
5	2323.024	0.007434	0.000161	0.000127	0.000499
6	2617.116	0.027249	0.000851	0.001733	0.001803
7	2890.739	0.012221	0.000145	0.000345	0.000782
8	3236.238	0.031371	0.002148	0.002303	0.002477
9	3314.401	0.034157	0.001268	0.002736	0.002295
10	3516.025	0.022258	0.000857	0.001152	0.001531
11	3765.953	0.036047	0.002215	0.003051	0.002749
12	4016.542	0.059318	0.002720	0.008393	0.003976
13	4281.442	0.032507	0.001957	0.002475	0.002427
14	4466.175	0.025621	0.000970	0.001530	0.001756
15	4547.503	0.039457	0.001371	0.003664	0.002678
16	4681.169	0.074505	0.004553	0.013376	0.005127
17	4776.150	0.050716	0.002683	0.006100	0.003640
18	5157.877	0.049048	0.002592	0.005699	0.003541
19	5306.036	0.054977	0.003720	0.007188	0.004233
20	5347.399	0.080702	0.005066	0.015758	0.005075
21	5616.426	0.065302	0.003547	0.010213	0.004459
22	5771.265	0.060528	0.004610	0.008746	0.004905
23	5835.224	0.062804	0.003832	0.009431	0.004267
24	6021.726	0.108558	0.010814	0.029043	0.007910
25	6034.291	0.061674	0.003399	0.009087	0.004133
26	6334.453	0.056232	0.003108	0.007527	0.003898
27	6471.491	0.085866	0.007258	0.017901	0.006564

FR, natural frequency computed with the actual model; PHE, percentage of higher order elastic energy computed with the actual model; EEE, elastic energy error computed by mesh halving; SEEE, standard elastic energy error; PHE REF, percentage of higher order elastic energy computed by mesh halving.

Table 10: Cast iron Cook's membrane. Estimation of the discretization error. Modes 1-27.

From Tables 7-10 it is observed that the percentage of higher order elastic energy decreases as the mesh is refined. Then, this energy component behaves as a modal error indicator. This result is consistent with the one obtained by the numerical dispersion analysis carried out for harmonic waves. From Fig. 10, 12, 14 and 16 and Tables 7-10 it is also observed that the standard modal elastic energy error SEEE and the modal elastic energy error EEE exhibit a similar evolution pattern as the modal order increases. Moreover, the standard modal elastic energy error SEEE generally overestimates the modal elastic energy error EEE, at least in the range of error that interests us. Typically it is considered that an elastic energy error around one per cent is an optimum upper bound to properly capture the elastic modes, at least from the engineering point of view. Then, by the standard modal elastic energy error SEEE, the accuracy of the modes computed can be confidently verified in order to select a cutoff modal order. It is

lastly observed that for the Cook's membrane the standard modal elastic energy error SEEE and the modal elastic energy error EEE generally vary in the same direction for each natural mode computed as the Poisson´s ratio increases; therefore, the proposed error indicator SEEE is suitably sensitive to the effect of the material properties on the modal error.

MODES	FR (Hz)	PHE	EEE	SEEE	PHE REF
1	496.825	0.013896	0.001554	0.000457	0.001366
2	1299.225	0.006981	0.000579	0.000115	0.000605
3	1525.337	0.013208	0.001712	0.000412	0.001346
4	2621.953	0.021676	0.001582	0.001117	0.001765
5	3316.006	0.008104	0.000215	0.000155	0.000553
6	3711.761	0.026722	0.000836	0.001704	0.001769
7	4139.941	0.012694	0.000288	0.000381	0.000850
8	4598.899	0.028562	0.001918	0.001949	0.002272
9	4714.153	0.037807	0.001399	0.003437	0.002507
10	5012.325	0.022241	0.001002	0.001176	0.001579
11	5355.102	0.037627	0.002197	0.003404	0.002832
12	5711.405	0.058959	0.002704	0.008481	0.003944
13	6130.546	0.033280	0.002122	0.002655	0.002510
14	6350.745	0.030508	0.001772	0.002226	0.002225
15	6520.358	0.042348	0.001459	0.004325	0.002882
16	6665.786	0.065685	0.003746	0.010574	0.004400
17	6737.023	0.052695	0.002946	0.006745	0.003820
18	7391.597	0.059764	0.003599	0.008719	0.004469
19	7478.430	0.061825	0.004199	0.009343	0.004203
20	7643.847	0.064297	0.004055	0.010123	0.004313
21	8003.109	0.071005	0.004628	0.012401	0.005018
22	8200.629	0.067451	0.004998	0.011164	0.005142
23	8318.532	0.054716	0.002930	0.007283	0.003911
24	8501.179	0.102405	0.009854	0.026346	0.007283
25	8579.712	0.066478	0.004259	0.010837	0.004464
26	9042.387	0.058784	0.003984	0.008429	0.004279
27	9176.123	0.087652	0.007354	0.019112	0.006520

Table 10 (cont.): Steel Cook's membrane. Estimation of the discretization error. Modes 1-27.

4 CONCLUSIONS

This paper studies the propagation of time-harmonic elastic waves in homogeneous and isotropic solid media discretized by energy-orthogonal finite elements. In this formulation the element stiffness matrix is split into basic and higher order components which are related to the mean and deviatoric components of the element strain field, respectively. This decomposition is applied both to the stiffness matrix and to the elastic energy of the finite element assemblage. Both plain-strain solids and generalized plain-stress plates are considered. The research is focused on the properties of the higher order elastic energy as an error indicator. The noteworthy conclusions of this paper are:

- By a dispersion analysis of plane harmonic waves an averaged correlation between the percentage of higher order elastic energy and the elastic energy error is yielded versus the Poisson´s ratio for both longitudinal waves and shear waves. Both the longitudinal wave correlation and the shear wave correlation are highly depended on the element considered, the quadrilateral with eight nodes and the triangle with six nodes, and clearly take into account the effect of dilatational locking for the almost incompressible plain-strain solids.
- The use of both the longitudinal wave correlation and the shear wave correlation as reference to apply the higher order elastic energy as an error indicator for the elastic vibration modes computed by the finite element method is explored. For both plain strain-solids and generalized plain-stress plates discretized by quasi-regular meshes, the numerical research reveals that by averaging both correlations the accuracy of the finite element model can be confidently verified in order to select a cutoff modal order for moderate values of elastic energy error.

The application of the proposed procedure to more complex media is subject of research.

MODES	FR (Hz)	PHE	EEE	SEEE	PHE REF
1	119.392	0.014148	0.001988	0.000491	0.001537
2	309.871	0.007537	0.000599	0.000139	0.000647
3	366.925	0.013087	0.002007	0.000420	0.001448
4	622.153	0.021519	0.001625	0.001142	0.001775
5	789.232	0.009151	0.000283	0.000205	0.000632
6	878.453	0.025972	0.000830	0.001669	0.001720
7	993.969	0.014688	0.000870	0.000529	0.001149
8	1092.650	0.025671	0.001288	0.001630	0.001906
9	1120.384	0.040136	0.001654	0.004026	0.002684
10	1199.901	0.022931	0.001114	0.001298	0.001651
11	1269.524	0.038641	0.002172	0.003728	0.002870
12	1354.212	0.058034	0.002736	0.008523	0.003886
13	1472.601	0.040264	0.002631	0.004052	0.002992
14	1498.577	0.035235	0.002440	0.003092	0.002640
15	1570.434	0.059941	0.003399	0.009105	0.004222
16	1584.053	0.055970	0.003192	0.007916	0.004007
17	1608.071	0.036834	0.001445	0.003383	0.002379
18	1755.181	0.050535	0.002996	0.006429	0.003681
19	1762.480	0.087788	0.006413	0.019908	0.006018
20	1844.355	0.052128	0.003584	0.006849	0.003706
21	1892.027	0.076996	0.006096	0.015201	0.005690
22	1956.401	0.068711	0.004269	0.012037	0.004927
23	1988.611	0.079723	0.007608	0.016327	0.006424
24	2007.375	0.074984	0.005219	0.014397	0.004511
25	2041.420	0.068488	0.005004	0.011957	0.004705
26	2152.557	0.073579	0.006975	0.013849	0.005699
27	2186.479	0.104824	0.010685	0.028714	0.008277

Table 10 (cont.): Lead Cook's membrane. Estimation of the discretization error. Modes 1-27.

REFERENCES

[1] F.J. Fahy, *Sound and structural vibration: radiation, transmission and response.* Academic Press, 1985.

[2] J.D. Achenbach, *Wave propagation in elastic solids.* Elsevier, 1975.

[3] K.F. Graff, *Wave motion in elastic solids.* Dover Publications, 1991.

[4] H.L. Schreyer, Dispersion of semidiscretized and fully discretized systems. T. Belytschko, T.J.R. Hughes eds. *Computational methods for transient analysis*. Elsevier Science, 1983.

[5] M. Okrouhlík, Computational aspects of stress wave problems in solids. *European Conference on Computational Mechanics (ECCM-2001),* Cracow, Poland, June 26-29, 2001.

[6] R. Kolman, J. Plešek, M. Okrouhlík, D. Gabriel, Grid dispersion analysis of plane square biquadratic serendipity finite element in transients elastodynamics. *International Journal for Numerical Methods in Engineering,* **96**, 1-28, 2013.

[7] R. Kolman, J. Plešek, M. Okrouhlík. Complex wavenumber Fourier analysis of the B-spline based finite element method. *Wave Motion,* **51**, 348-359, 2014.

[8] Ben-Menahem, S.J. Singh, *Seismic waves and sources.* Dover Publications, 2000.

[9] H.J.-P. Morand, R. Ohayon, *Fluid structure interaction,* John Wiley, 1995.

[10] C.A. Felippa, B. Haugen, C. Militello, From the individual element test to finite element templates: evolution of the Patch Test. *International Journal for Numerical Methods in Engineering*, **38**, 199-229, 1995.

[11] P.G. Bergan, M.K. Nygärd, Finite elements with increased freedom in choosing shape functions. *International Journal for Numerical Methods in Engineering*, **20**, 643-664, 1984.

[12] C.A. Felippa, A survey of parametrized variational principles and applications to computational mechanics. *Computer Methods in Applied Mechanics and Engineering*, **113**, 109-139, 1994.

[13] F.J. Brito Castro, Dispersion analysis of acoustic waves in fluid media discretized by energy-orthogonal finite elements. M. Papadrakakis, V. Papadopoulos, V. Plevris eds. *5th ECCOMAS Thematic Conference on Computational Methods in Structural Dynamics and Earthquake Engineering (COMPDYN 2015),* Crete Island, Greece, May 25–27, 2015.

[14] O.C. Zienkiewicz, R.L. Taylor, *Finite element method, Vol. 1.* Butterworth-Heinemann, 2000.

[15] S.I. Rokhlin, D.E. Chimenti, P.B. Nagy, *Physical ultrasonics of composites.* Oxford University Press, 2011.

[16] M. Okrouhlík, C. Höschl, A contribution to the study of dispersive properties of one-dimensional lagrangian and hermitian elements. *Computers and Structures*, **49**, 779-795, 1993.

[17] W.H. Press, S.A. Teukolsky, W.T. Vetterling, B.P. Flannery, *Numerical recipes in fortran.* Cambridge University Press, 1992.

[18] L. Brillouin, *Wave propagation in periodic structures.* Dover Publications, 2003.

[19] J. Barlow, More on optimal stress points-reduced integration, element distortions, and error estimation. *International Journal for Numerical Methods in Engineering*, **28**, 1487-1504, 1989.

[20] R.H. MacNeal, *Finite elements: their design and performance.* Marcel Dekker, 1994.

[21] K.J. Bathe, *Finite element procedures.* Prentice Hall, 1996.

[22] J.N. Reddy, *Applied functional analysis and variational methods in engineering.* Krieger Publishing Company, 1986.

[23] M. Petyt, *Introduction to finite element vibration analysis.* Cambridge University Press, 2010.

[24] G.R. Liu, *Mesh free methods: moving beyond the finite element method.* CRC Press, 2003.

[25] R. Cook, Improved two-dimensional finite element. *Journal of the Structural Division*, ASCE 100; ST6: 1851-1863, 1974.